

Article

Sorption Thermodynamics of CO₂, H₂O, and CH₃OH in a Glassy Polyetherimide: A Molecular Perspective

Giuseppe Mensitieri ^{1,2,*} , Giuseppe Scherillo ¹ , Pietro La Manna ² and Pellegrino Musto ²

¹ Department of Chemical, Materials and Production Engineering, University of Naples Federico II, Piazzale Tecchio 80, 80125 Naples, Italy; gscheril@unina.it

² Institute for Polymers, Composites and Biomaterials, National Research Council of Italy, Viale Campi Flegrei 34, 80078 Pozzuoli (Na), Italy; pietro.lamanna@unina.it (P.L.M.); pellegrino.musto@cnr.it (P.M.)

* Correspondence: mensitie@unina.it; Tel.: +39-081-7682512

Received: 15 November 2018; Accepted: 18 January 2019; Published: 1 February 2019



Abstract: In this paper, the sorption thermodynamics of low-molecular-weight penetrants in a glassy polyetherimide, endowed with specific interactions, is addressed by combining an experimental approach based on vibrational spectroscopy with thermodynamics modeling. This modeling approach is based on the extension of equilibrium theories to the out-of-equilibrium glassy state. Specific interactions are accounted for in the framework of a compressible lattice fluid theory. In particular, the sorption of carbon dioxide, water, and methanol is illustrated, exploiting the wealth of information gathered at a molecular level from Fourier-transform infrared (FTIR) spectroscopy to tailor thermodynamics modeling. The investigated penetrants display a different interacting characteristic with respect to the polymer substrate, which reflects itself in the sorption thermodynamics. For the specific case of water, the outcomes from molecular dynamics simulations are compared with the results of the present analysis.

Keywords: glassy polymers; sorption thermodynamics; lattice fluid theory; polyetherimide; carbon dioxide; water; methanol

1. Introduction

Sorption thermodynamics of low-molecular-weight compounds within synthetic polymers, as well as the associated interactional issues, is a subject of considerable technological and fundamental interest, as proven by the recent literature reporting on experimental characterization techniques, theoretical approaches, and molecular simulations [1–13]. Sorption of gases and vapors in polymers has important technological implications as, for example, durability of polymer matrices for composites [14], membranes for separation of liquid and gaseous mixtures [15–18], and barrier polymers for packaging applications [19].

Depending on the chemical structure of the polymer and the penetrant, the system can be endowed with specific interactions, such as hydrogen bonding or other acid–base type interactions. We previously investigated and theoretically modeled sorption thermodynamics of gases and vapors in glassy polymers characterized by different levels of interactions [20–23] by complementing the theoretical modeling with the wealth of information gathered from vibrational spectroscopy and gravimetric measurements. These techniques provided a comprehensive molecular characterization of the systems under scrutiny, which was used to tailor the structure of the model. In detail, the experimental results were successfully interpreted using the so-called non-equilibrium theory for glassy polymers with non-random hydrogen bonding (NETGP-NRHB) [22], a model based on a compressible lattice fluid framework which is able to account both for the specific interactions and the non-equilibrium nature of glassy polymers. This approach is based on an extension of the equilibrium NRHB equation of state (EoS) theory [24,25], originally developed by Panayiotou et al. to deal with

rubbery polymers. This extension was performed following the procedure introduced by Sarti and Doghieri [26,27].

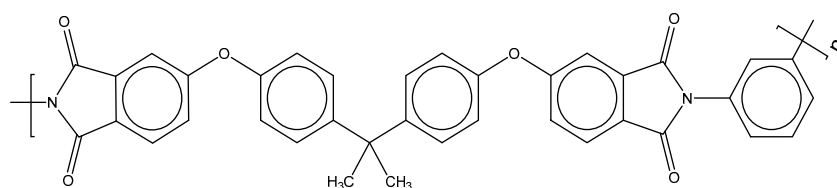
Polyimides find relevant applications as membrane materials in view of their permeability and selectivity properties, as well as of their strong resistance to organic solvents [28]. Polyetherimide (PEI) belongs to this class of polymers. It is an amorphous engineering thermoplastic with a relatively high glass transition temperature ($\cong 216$ °C), a chain flexibility provided by ether groups, and high heat resistance imparted by aromatic imide groups. Thanks to its excellent chemical, mechanical, thermal, and transport properties, and to its durability [29–31], it is the material of choice for several separation processes [19,32–35]. Understanding at a molecular level the interactions between polymer backbone and penetrants is crucial for the optimal design of separation processes. In particular, hydrogen-bonding (HB) interactions significantly affect membrane mass transport and separation performances in those processes involving water and alcohols [36–45].

We present here a theoretical analysis of the sorption of low-molecular-weight penetrants in PEI combined with experimental investigations. The present contribution puts together unpublished results on the CO₂–PEI system with results on the H₂O–PEI and CH₃OH–PEI systems obtained by our group and already reported in recent publications [20,46–48]. The aim was to compare the thermodynamic behavior of systems displaying widely different interactive characteristics. As anticipated, non-equilibrium lattice fluid models are combined with Fourier-transform infrared (FTIR) spectroscopy and gravimetric analyses. Information gathered from the experiments was used to identify the involved interactions to be accounted for in the modeling and to validate model predictions. A rather clear physical picture emerged on self- and cross-interactions, providing quantitative and qualitative indications on the involvement of the moieties present on the polymer backbone.

2. Materials and Methods

2.1. Materials

Totally amorphous PEI (see Scheme 1) was a commercial-grade product, kindly supplied by Goodfellow Co., PA, USA, in the form of a 50.0- μ m-thick film. To obtain film thicknesses suitable for FTIR spectroscopy, the original product was first dissolved in chloroform (15% *w/w* concentration) and then cast onto a tempered glass support. The solution was spread using a calibrated Gardner knife, which allows one to control the film thickness in the range of 10–70 μ m. The cast film was dried 1 h at room temperature and 1 h at 80 °C to allow most of the solvent to evaporate, and at 120 °C under vacuum over night. At the end of the drying protocol, the film was removed from the glass substrate by immersion in distilled water at 80 °C.



POLYETHERIMIDE

Scheme 1. Chemical structure of PEI.

Thinner films (1.0–3.0 μ m) were prepared via a two-step, spin-coating process performed with a Chemat KW-4A apparatus from Chemat Technologies Inc (Northridge, CA, USA). Spinning conditions were 12 s at 700 rpm for the first step and 20 s at 1500 rpm for the second step. The spin-coated films were dried in the same conditions as for the thicker films, and freestanding samples were removed in distilled water at room temperature.

Methanol used for sorption experiments was purchased from Sigma-Aldrich (Milano, Italy) with purity higher than 99.6%. Deionized water was used for water vapor sorption experiments. Before use,

both water and methanol were degassed through several freezing–thawing cycles. CO₂ with a purity of 99.5% was purchased from Linde, Germany.

2.2. Gravimetric Measurements

The apparatus used to determine the sorption isotherms in PEI was based on the measurement of the elongation of a calibrated quartz spring microbalance (see Figure 1). The microbalance system recorded the weight gain of a sample exposed to a controlled environment (temperature and pressure of gaseous CO₂ or of water and methanol vapor). The quartz spring was placed in a water-jacketed glass cell that was connected, through service lines, to a CO₂ cylinder or to a water or methanol reservoir, to a turbo-molecular vacuum pump, and to pressure transducers. The polymer sample hung from the hook of the quartz spring. Changes in weight of the sample determined by sorption of the penetrant brought about the elongation of the spring that was monitored using a traveling camera, equipped with a macro objective, screwed on a computer-controlled piezoelectric slide. The microbalance provided a sensitivity of 1.0 µg with an accuracy of ±2.0 µg.

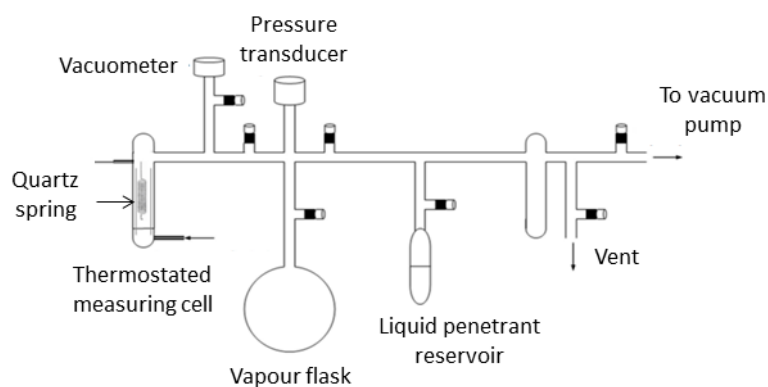


Figure 1. Schematic representation of quartz spring sorption apparatus in the configuration for vapour sorption. In the case of gas sorption, a penetrant reservoir is substituted by service lines to the gas cylinder. The polyetherimide (PEI) film sample hangs from the quartz spring located in the measuring cell.

Gravimetric sorption isotherms were collected at 18, 27, and 35 °C in the case of CO₂, at 30, 45, 60, and 70 °C in the case of water, and at 30 °C in the case of methanol. Sorption tests were performed starting from neat polymer by increasing the pressure of penetrant in a stepwise manner, waiting for the attainment of a constant weight at each step. Full details about the experimental procedure are given elsewhere [20–22].

2.3. In Situ FTIR Spectroscopy

Spectroscopic analysis of sorption processes was performed by time-resolved acquisition of the spectra of polymer films exposed to gaseous carbon dioxide or water and methanol vapors, at a constant pressure. These measurements were carried out in the transmission mode, and sorption kinetics was monitored up to the attainment of equilibrium.

The spectroscopic set-up consisted of a diffusion cell placed in the sample compartment of a suitably modified FTIR spectrometer. In the case of CO₂ sorption, the tests were performed with flowing gas. A schematic view of the apparatus is reported in Figure 2. The cell was connected to a gas line where the flux was regulated by a mass-flow controller and the downstream pressure was controlled by a solenoid valve. The cell temperature could be controlled between –190 °C and 350 °C. Differential sorption tests at 35 °C were performed by increasing stepwise the CO₂ pressure within the 40–150 Torr range.

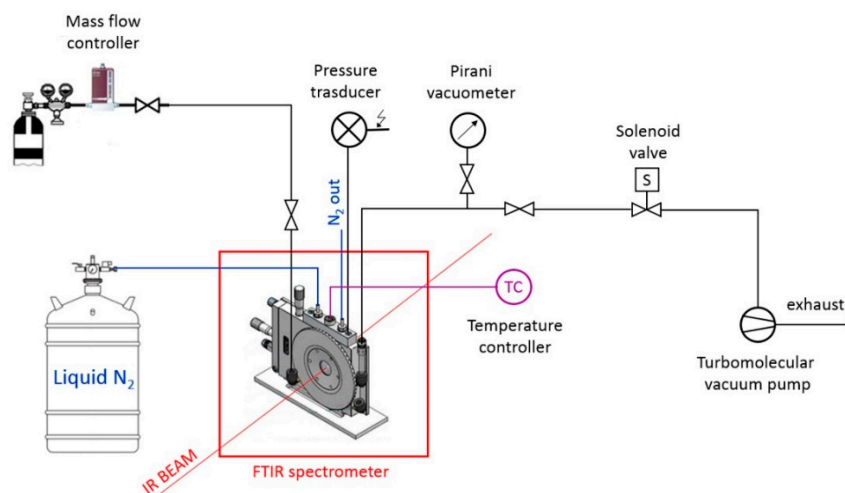


Figure 2. Schematic representation of experimental apparatus for Fourier-transform infrared (FTIR) spectroscopy measurements of CO₂ sorption. The PEI film sample is located inside the test cell, normally to the IR beam of the FTIR spectrometer.

In the case of water and methanol vapors, the tests were performed in static conditions. A custom-designed vacuum-tight FTIR cell was used to acquire the time-resolved FTIR spectra during the sorption experiments (see Figure 3). The cell, whose temperature could be controlled between $-20\text{ }^{\circ}\text{C}$ and $120\text{ }^{\circ}\text{C}$, positioned in the sample compartment of the spectrometer, was connected through service lines, to a water or methanol reservoir, a turbo-molecular vacuum pump, and pressure transducers. Full details of the experimental set-up are reported in References [49,50]. Before each sorption measurement, the sample was dried under vacuum overnight at the test temperature in the same apparatus used for the test. Differential sorption tests at $30\text{ }^{\circ}\text{C}$ were performed by increasing stepwise the relative pressure of the vapor, p/p_0 (where p is the pressure of the vapor and p_0 is the vapor pressure at the test temperature), within the 0.0–0.6 range.

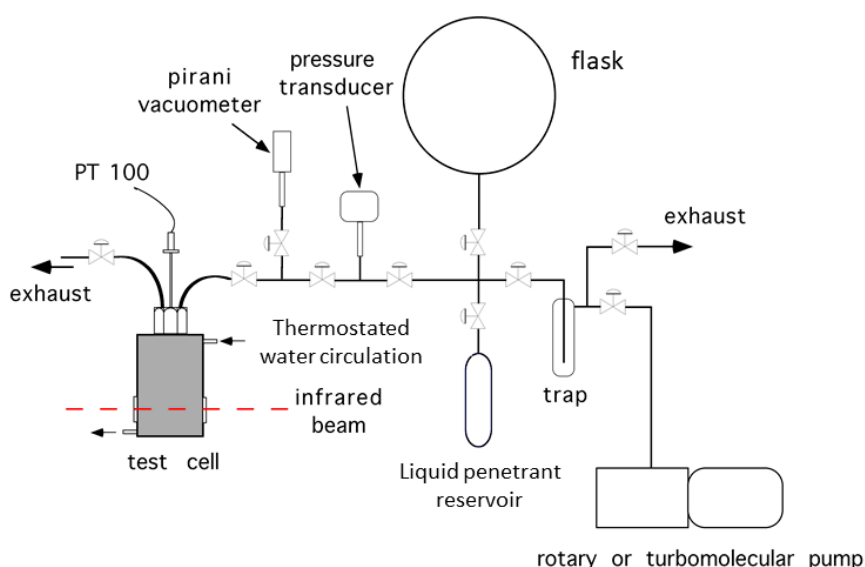


Figure 3. Schematic representation of experimental apparatus for FTIR measurements of H₂O and methanol vapor sorption. The PEI film sample is located inside the test cell, normally to the IR beam of the FTIR spectrometer.

Spectra were collected using a Spectrum 100 FTIR spectrometer (PerkinElmer, Norwalk, CT, USA), equipped with a Ge/KBr beam splitter and a wide-band deuterated triglycine sulfate (DTGS) detector.

The spectral resolution was set to 2 cm^{-1} , with an optical path difference (OPD) velocity of 0.5 cm/s . Collection time for a single spectrum was 2.0 s . Spectra were collected and stored for further processing in the single-beam mode. A dedicated software package was employed to control automated data acquisition (*Timebase* from Perkin-Elmer).

The cell without sample, at the test conditions, was used as background to obtain full absorbance spectra (i.e., polymer plus sorbed compound). The spectra representative of the different penetrants were isolated by difference spectroscopy (DC), which allowed us to eliminate the interference of the polymer substrate.

$$A_d(\nu) = A_s(\nu) - kA_r(\nu),$$

where ν is the frequency, and $A_d(\nu)$, $A_s(\nu)$, and $A_r(\nu)$ are, respectively, the difference spectrum (the sorbed penetrant), the sample spectrum (the polymer containing the sorbed penetrant), and the reference spectrum (the dry polymer). The subtraction factor, k , allows to compensate for changes in the optical path (sample thickness) resulting from possible swelling. In the present cases, it was verified by spectroscopic means that a negligible volume change occurred; hence, a k value of 1 was consistently taken.

In the transmission FTIR measurements, sample thickness could be used to adjust the sensitivity, provided that the polymer substrate made no or limited interference in the frequency range where the relevant signals of the penetrant spectrum were located. Obviously, the sensitivity increment was achieved at the expense of the time to equilibration, and a trade-off was established between sensitivity and experiment duration. For this reason, thick samples ($40\text{--}60\ \mu\text{m}$) were used to monitor the spectrum of the penetrant, whose concentration was very low, thus achieving an optimum signal-to-noise ratio. Conversely, to investigate the effect of the penetrant on the polymer spectrum, thin films were used ($1\text{--}3\ \mu\text{m}$) that allowed keeping the intense carbonyl bands of PEI in the range of linearity of the absorbance vs. concentration curve.

3. Theoretical Background: Modeling of Sorption Thermodynamics

Sorption thermodynamics of low-molecular-weight compounds in glassy polymers was addressed using different approaches, some of which account for the molecular details associated with this process. In fact, there are various sorption modes, occurring simultaneously, that should be considered in modeling sorption equilibria: bulk dissolution and specific interactions (including self and cross hydrogen bonding, Lewis acid/Lewis base interactions, and penetrant clustering). Another relevant issue, when dealing with glassy polymers, is their non-equilibrium nature. In this section, we provide an overview of some significant lattice fluid modeling approaches proposed in the literature to interpret sorption thermodynamics in rubbery and glassy polymers. The reader is referred to Appendix A for the mathematical details of some theoretical approaches relevant in the present context.

In the last four decades, EoS-based theoretical models were introduced to address equilibrium thermodynamics of rubbery polymer–penetrant mixtures, possibly accounting for the occurrence of specific interactions (e.g., hydrogen bonding (HB) and Lewis acid/Lewis base interactions). Sorption thermodynamics in glassy polymers, endowed or not with specific interactions, was successfully interpreted by properly extending the equilibrium models, originally developed to describe sorption thermodynamics in rubbery polymers, to the case of polymers in an out-of-equilibrium glassy state.

The compressible lattice fluid (LF) model proposed by Sanchez–Lacombe (SL) [51–53] is one of the early examples of EoS-based approaches that were developed to describe sorption in rubbery polymers. Such a model assumes that a random mixing occurs within the polymer–penetrant mixture. The lattice fluid framework for fluid mixtures takes each component (i.e., polymer and low-molecular-weight penetrant in the present context) as consisting of a series of chemically bonded n -mers, each one accommodated in a cell of the lattice. Since the lattice is compressible, not all the cells are occupied by the n -mers, some of them being possibly empty (holes). Chemical bonds are established between first neighbor n -mers belonging to the same molecule, but contacts are also established with other non-bonded n -mers located in adjacent first-neighbor cells. The coordination number, z , which is

a parameter of the model lattice, rules the number of contacts between first-neighbor cells. Contacts established between *r*-mers of the same type are named homogeneous; otherwise, they are said to be heterogeneous. Sorption equilibrium in binary systems is ruled by the equivalence of chemical potentials of each component in the two phases in contact, i.e., the polymer–penetrant mixture and the gaseous phase. The SL theory provides the expressions for the chemical potentials of each of the mixture components, as well as the expression of the equations of state of the mixture and of each pure component. Since it is generally assumed that no polymer is present in the gaseous phase, the equivalence is only imposed to the chemical potentials of the penetrant in the two phases in contact. Densities of the two phases in contact are provided by the EoS of each phase. Parameters of the model are the three scaling parameters of the EoS for the two pure components and the value of the binary interaction parameter that is related to the energy associated to formation of heterogeneous contacts occurring between the *r*-mers of the two components in a binary mixture and the energy associated to the formation of homogeneous contacts between the *r*-mers of each component.

Later, lattice fluid theories were further developed to describe sorption of low-molecular-weight compounds in rubbery polymers for systems endowed with HB interactions. These approaches were developed by properly modifying available LF models that account only for mean field interactions to include the effect of occurrence of self and cross hydrogen bonding. Worthy of mention is the model proposed by Panayiotou and Sanchez (PS) [54] that, starting from the original Sanchez–Lacombe theory, introduced additional terms accounting for the formation of HB interactions. A key assumption in this development was the factorization of the configurational partition function in two separate contributions, respectively associated with mean field interactions and to specific interactions. The PS model, in fact, combines the SL mean field contribution with an HB contribution formulated on the basis of a combinatorial approach first proposed by Veytsman [55,56]. This model requires, in addition to the parameters already mentioned in the case of SL theory, the HB interaction parameters associated with each type of proton donor–proton acceptor adduct that can be formed in the system.

A remarkable intrinsic simplification of the SL model, as well as of the related PS model, is that the evaluation of the mean field contribution is, in both cases, based on a random arrangement of *r*-mers and holes in the lattice. This assumption is that a more inappropriate arrangement suggests a greater number of non-athermal contacts occurring between different kinds of *r*-mers [57]. Several approaches were then proposed to account for possible non-random distribution of contacts by following the pioneering work of Guggenheim [58]. As a first step, systems without specific interactions were addressed. Also in this case, the assumption was that the partition function can be factorized, in an ideal random contribution and in a non-random contribution “correction term”. The latter was formulated considering the establishment of each contact as a reversible chemical reaction (the so-called “quasi-chemical approximation”). The original development proposed by Guggenheim was based on a lattice fluid system without holes, but Panayiotou and Vera (PV) improved this theory by introducing a compressible LF model (i.e., with the presence of hole sites) [59]. In the PV model, only contacts between *r*-mers of the mixture components were non-random, while the hole site distribution was still random. Later, You et al. [60] and Taimoori and Panayiotou [61] further upgraded this approach introducing the non-randomness of all the possible couples of contacts, still adopting a non-random quasi-chemical approximation.

A further step consisted in the formulation of an LF-EoS theory accounting both for the occurrence of specific interactions and for the non-randomness of distribution of contacts within the lattice. In fact, Yeom et al. [62] and Panayiotou et al. [2,24,25,63,64] modified the PV approach to include the contribution of HB interactions. Again, the key assumption was the factorization of the configurational partition function in different terms: a mean field random term, a non-randomness “correction term”, and a term accounting for specific interactions. In the present context, the non-random model is of particular interest, which also accounts for cross and self HB interactions, proposed by the group of Panayiotou in References [2,24,25]. We refer to this theory hereafter as the “non-random lattice fluid hydrogen bonding” (NRHB) model. The theory can be used to calculate the chemical potential of

the polymer and of the penetrant, both in the polymer mixture and in the vapor or gaseous phase in equilibrium with it, as well as the EoS of both phases. The types of parameters required to perform calculations are similar to those required in the case of PS model. Examples of good correlations of the experimental sorption isotherms using the NRHB model were provided by Tsivintzelis et al. [65] for the case of mixtures of poly(ethylene glycol), poly(propylene glycol), poly(vinyl alcohol), and poly(vinyl acetate) with several solvents, including water.

The theories discussed so far are well suited to describe the sorption behavior of rubbery polymers. When dealing with modeling of sorption thermodynamics in a glassy polymer, one has to tackle an additional complexity, i.e., the non-equilibrium nature of the glassy state. Rational non-equilibrium thermodynamics provides an adequate theoretical framework to address this issue. In fact, using a proper reformulation, it is possible to extend the equilibrium theories developed for mixture thermodynamics—adequate for describing sorption thermodynamics in rubbery polymers—to the case of sorption in glassy polymers. This procedure is based on thermodynamics endowed with internal state variables. Order parameters that mark the departure, at a certain pressure and temperature, from the equilibrium conditions, are selected to play the role of internal state variables. In fact, in addition to the external state variables, which are the only ones needed to describe the state of a system at equilibrium (e.g., pressure, temperature, and concentration), a set of order parameters are used as internal state variables to provide a proper interpretation of the state of non-equilibrium glassy polymer–penetrant mixtures. This line of thought was introduced by Sarti and Doghieri [26,27], which adopted the density of the polymer in the mixture as the only order parameter and internal state variable. These authors introduced a procedure that enables the extension to non-equilibrium glassy systems of several equilibrium statistical thermodynamics mixture theories (in Appendix A, some further details are provided). This approach, referred to as “non-equilibrium thermodynamics for glassy polymers” (NETGP) [66], was demonstrated to be very effective in describing the thermodynamics of numerous binary and ternary glassy polymer–penetrant mixtures. A relevant difficulty that one encounters when applying this theory is that the expression for evolution kinetics of the internal state variable has to be known. To avoid dealing with complex evolution kinetics of non-equilibrium polymer density, a “simplified” version of this approach considers the polymer as being “frozen” in a kinetically locked pseudo-equilibrium (PE) state. This assumption is legitimate for glassy polymers at temperatures well below their glass transition temperature and when the concentration of penetrant within the polymer phase is low. To deal with cases in which such conditions do not occur, the theory was properly formulated to take also into account the structural evolution of the glassy system during penetrant sorption. The NETGP approach requires the knowledge of the same parameters as for the equilibrium theory from which it is derived. The phase equilibrium is still dictated by the equivalence of chemical potentials of each component in the two phases. However, differently from the case of sorption in rubbery polymers, no equation of state can be written for the polymer phase. In fact, in the case of glassy polymers, the value of polymer density cannot be calculated using an equilibrium EoS, but is determined by its intrinsic evolution kinetics; its value, which is necessary to perform model calculations, should be known from independent experimental data. In particular, in the present context, we refer to the so called “non-equilibrium lattice fluid” (NELF) model [26,27] as the NETGP extension of the equilibrium Sanchez–Lacombe theory to treat sorption in glassy polymers not endowed with specific interactions (see Appendix A, for details).

To deal with sorption thermodynamics for glassy polymer–penetrant systems exhibiting specific interactions, extensions of equilibrium models able to cope with self- and cross-interactions were then proposed. Referring to the case of EoS-based models, of particular relevance are the extensions of “statistical associating fluid theory” (SAFT) [67] and NRHB [68] approaches. Our group developed and applied an extension of the NRHB model to non-equilibrium glassy polymers to account for HB interactions in water/glassy polymer mixtures [22]. We refer to this model here as NETGP-NRHB (see Appendix A for details). Again, this model requires the same parameters as for the equilibrium NRHB

model. In addition, the value of polymer density should also be known, since it cannot be provided by an EoS.

4. Results and Discussion

In this section, we discuss the results of experimental analysis and of theoretical modeling of the PEI-CO₂, PEI-water, and PEI-methanol systems. Results of in situ FTIR spectroscopy are presented along with their elaboration by means of two-dimensional correlation spectroscopy (2D-COS) [23,69–71]. Indications emerging from FTIR measurements were used to tailor the structure of sorption thermodynamics model, which was then used to fit gravimetric sorption isotherms.

4.1. PEI-CO₂ System

4.1.1. FTIR Analysis: Absorbance, Difference, and Two-Dimensional Correlation Spectra

As reported in Section 2.3, to achieve an optimum signal-to-noise ratio, thick samples were used to monitor the spectrum of the penetrant, whose concentration was very low. Conversely, to analyze the effect of the sorbed penetrant on the polymer spectrum, thin films were used in order to keep the relevant bands of PEI in the range of linearity of the absorbance vs. concentration curve. In Figure 4A, the spectra of a fully dried film (red trace) and of the same film equilibrated at 35 °C under a CO₂ pressure of 150 Torr (blue trace), collected on a 37.7- μm -thick film, are compared. This was the kind of sample used to perform the subtraction spectroscopy analysis on the spectral region populated by signals associated to penetrant molecules. In Figure 4B, the same comparison for the spectra collected on a much thinner film, with a thickness of 2.6 μm , is shown. This was the kind of sample used to perform the subtraction spectroscopy analysis in the spectral region with signals characteristic of the polymer, in order to detect possible perturbations related to the presence of sorbed CO₂. In particular, attention was focused on the intense carbonyl bands of PEI, and the thickness was selected to keep the associated absorbance vs. concentration curve in the range of linearity. It is worth noting that, in the case of the “thin” sample, the weakness of the penetrant signals, even at the maximum CO₂ pressure, did not allow a reliable band-shape analysis. Furthermore, the sorption kinetics was so fast that a time-resolved measurement and the associated two-dimensional correlation analysis (vide infra) were unfeasible.

It was immediately apparent, from the comparison of the two traces reported in Figure 4A, that sorbed carbon dioxide produced two signals, centered at 2336 and 655 cm^{-1} . The high-frequency band was due to the antisymmetric stretching mode (ν_3) at 2336 cm^{-1} plus a satellite peak at 2324 cm^{-1} . The latter component was a non-fundamental transition, in particular a hot band enhanced by Fermi resonance with the main stretching mode [72]. It is to be stressed that the peak at 2324 cm^{-1} was not due to a second CO₂ species, but to a further signal produced by the same species that generated the main absorption at 2336 cm^{-1} .

The ν_3 mode was well suited for quantitative analysis and for achieving information at the molecular level. The carbon dioxide bending mode (ν_2) found at around 655 cm^{-1} was less useful, being much weaker and superimposed onto intense polymer bands. The suppression of the polymer matrix interference by difference spectroscopy [50,69] allows one to isolate the spectrum of absorbed CO₂. The integrated absorbance of the 2336 cm^{-1} band was collected at each pressure as a function of sorption time up to attainment of sorption equilibrium.

In Figure 5A, the ν_3 band of CO₂ after sorption equilibrium at different pressures is reported. The correlation between integrated absorbance and gravimetric data, collected at 35 °C, at sorption equilibrium at different CO₂ pressures, is represented in Figure 5B. The behavior was linear through the origin, thus verifying the Lambert–Beer law, which allows one to convert the absorbance data into absolute concentration values. In the explored pressure range (40–160 Torr), the sorption isotherm was linear (see Figure 5C). The band-shape of the ν_3 mode was exactly coincident at all pressures (see

Figure 5A) indicating that, in the explored range, the molecular interactions formed with the polymer substrate did not depend on CO₂ concentration.

The time-resolved spectra were subjected to 2D-COS analysis, which is very effective for investigating molecular interactions [69]. This is a perturbative technique applied to systems that are initially at equilibrium; these are then subjected to an external stimulus and the spectral response of the system is treated by a correlation analysis. The covariance of two correlated signals (peak absorbance, in the present case) is measured as a function of a third common variable related to the perturbing function (time, in the present case). This procedure spreads the spectral data over a second frequency axis and allows unambiguous assignments through the correlation of bands. It produces synchronous and asynchronous maps. In the latter, the correlation intensity for signals evolving at the same rate vanishes [71], thus providing a resolution enhancement. Moreover, valuable dynamic information can be also gathered.

In Figure 6A,B, the synchronous spectrum in the 2250–2420 cm⁻¹ range, obtained from the time-resolved spectra collected during the sorption experiment at 150 Torr and 308 K, and the power spectrum, i.e., the autocorrelation profile taken across the main diagonal, are reported. The synchronous spectrum (Figure 6A) displays a highly characteristic cross-shape; in the power spectrum (Figure 6B), a strong auto-peak was detected at 2336 cm⁻¹, corresponding to the main component in the frequency spectrum, plus a weak, fully resolved feature at 2324 cm⁻¹. The off-diagonal wings present in the synchronous map (Figure 6A) extend by about 60 cm⁻¹ and reflect the presence of a further component, increasing on sorption or decreasing on desorption concurrently with the main peaks (at 2336 and 2324 cm⁻¹). The elongated shape of the off-diagonal feature indicated that this component was significantly broader than the main peaks.

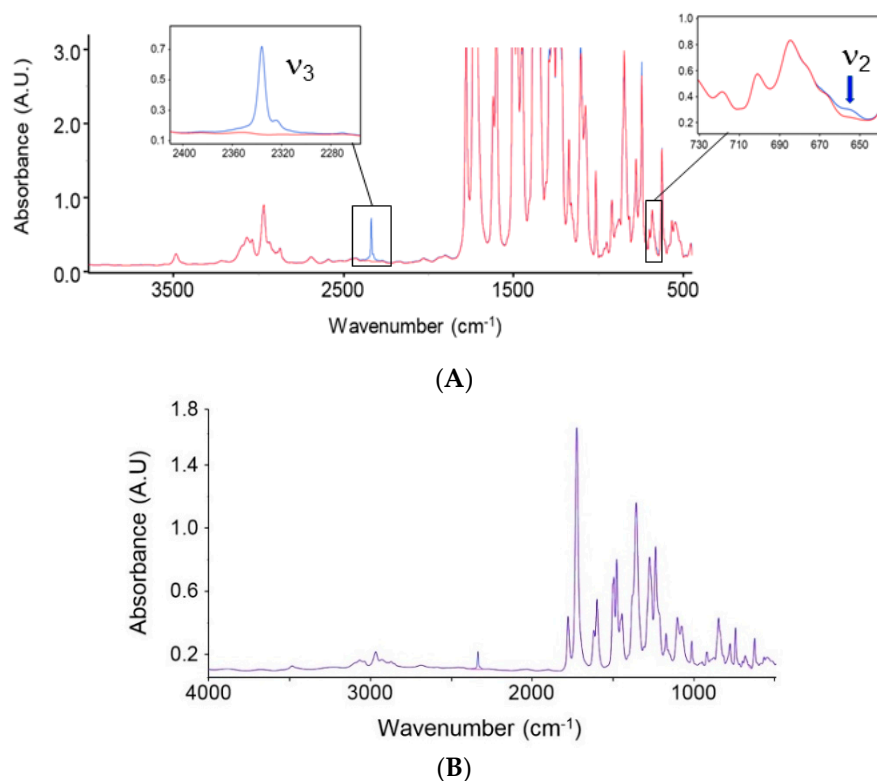


Figure 4. (A) Absorbance spectra of fully dried PEI (red trace) and PEI equilibrated at 35 °C at a CO₂ pressure of 150 Torr (blue trace). The insets highlight the bands of sorbed CO₂. The spectra were collected on a 37.7- μm -thick film. (B) Same as (A); measurement performed on a 2.6- μm -thick film.

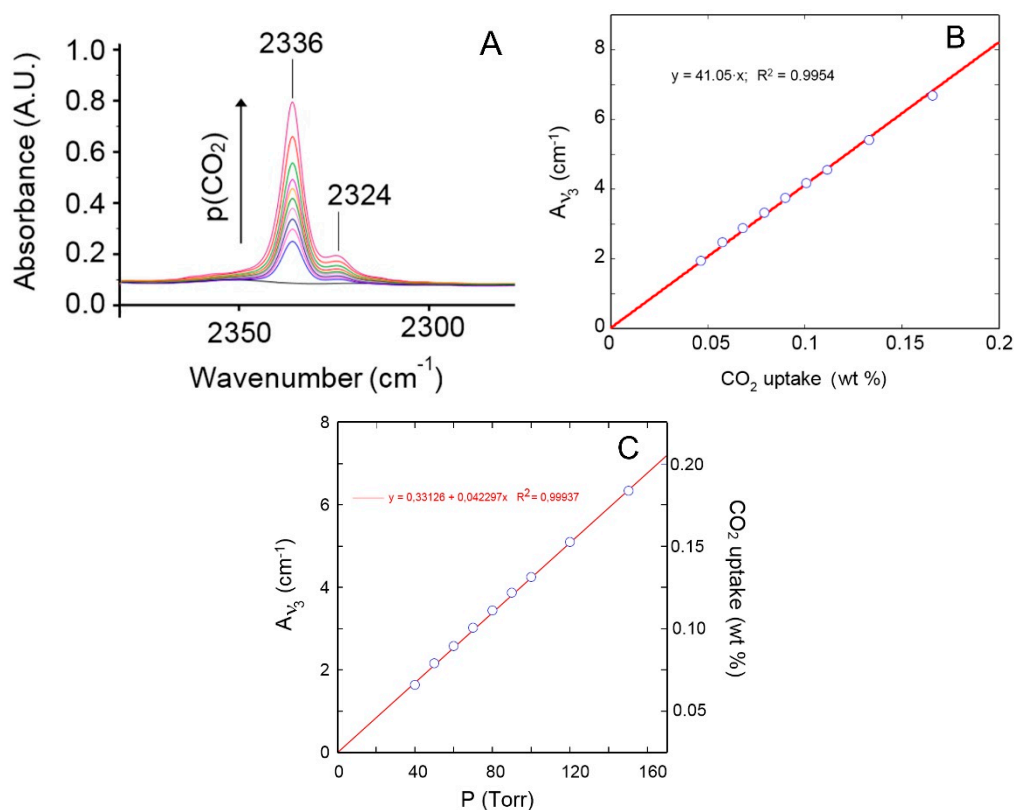


Figure 5. (A) The ν_3 band of CO_2 after sorption equilibrium at different pressures. (B) Absorbance of the ν_3 band as a function of sorbed CO_2 as evaluated gravimetrically at 35°C . (C) FTIR isotherm at 35°C . The right axis was obtained from the calibration curve of Figure 5B.

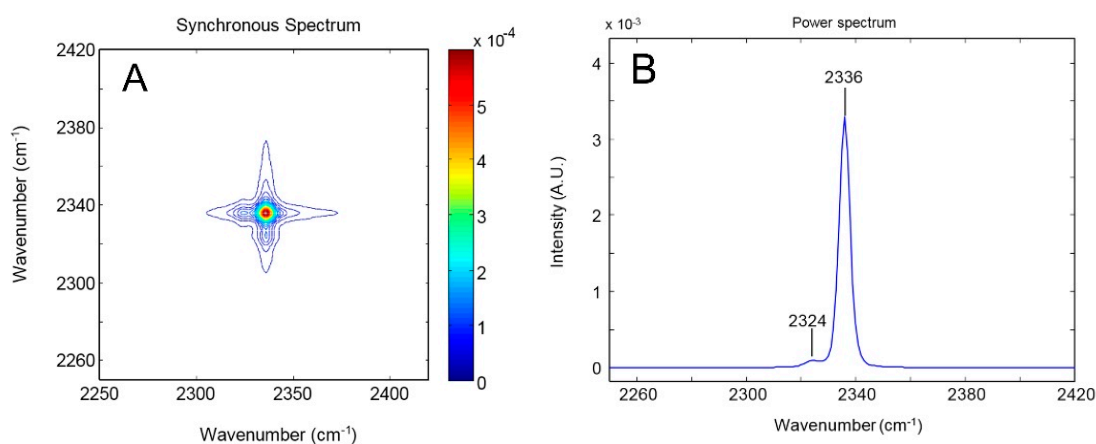


Figure 6. (A) Synchronous spectrum obtained from the time-resolved spectra collected during the sorption experiment performed at 150 Torr and at 35°C . (B) Power spectrum calculated therefrom.

The asynchronous spectrum was featureless (see Figure 7A,B). Only noise was present despite the significant intensity of the band and its complex structure. This result was relevant; it demonstrated that all the components in the ν_3 profile evolved synchronously, which, in turn, signified that the species they originated from had comparable dynamics or, alternatively, that a single molecular species produced all the observed components. Albeit no conclusive evidence is yet available, we are inclined toward the second hypothesis, in view of previous studies on solvated low-molecular-weight compounds [73,74].

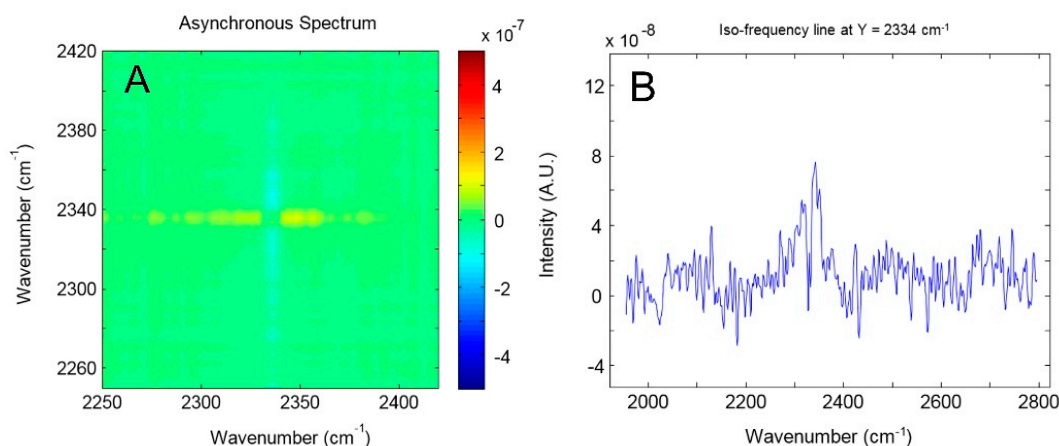


Figure 7. (A) Asynchronous spectrum obtained from the time-resolved spectra collected during the sorption experiment performed at 150 Torr and at 35 °C. (B) Iso-frequency profile at 2334 cm^{-1} .

Similar band profiles were reported in the literature (i.e., a broad Gaussian component superimposed onto a sharper peak of larger intensity) and were interpreted assuming the Gaussian part as being a remnant of the gas-phase spectrum, while the sharp, Lorentz-like component was interpreted as the purely vibrational transition active in the condensed phase (but not in the gas-phase) [73,74]. According to this interpretation, the two-component band-shape was the consequence of probe dynamics within the molecular environment (essentially free rotation in the early stages of the relaxation process, 0.2–1.0 ps), which produced the Gaussian part, and a random rotational diffusion regime at later stages (the so-called Debye regime), giving rise to the Lorentzian part. The band-shape models based on small-molecule mobility invariably tend to overlook the role played by molecular interactions. This is partially due to the difficulty in embracing the effects of specific contacts in a random collisional framework. In the present case, the specific interaction between CO_2 and PEI emerged clearly from the vibrational analysis (vide infra) and was taken into account when interpreting the band-shape and the 2D-COS results. Our view is that the probe molecules sorbed in PEI were characterized by very short free-rotation regimes (the Gaussian component is barely detectable in the frequency spectrum); the main component was due to a single molecular species of CO_2 forming a specific type of interaction with the polymer substrate. The uniqueness of the interaction is suggested by the sharp and highly symmetrical nature of the main ν_3 component, coupled with the absence of asynchronous features in the 2D-COS map. Work is in progress to substantiate this hypothesis and to put the above considerations on more quantitative grounds.

To complete the characterization of the probe-to-substrate interaction, we had to recognize the functional group(s) of the PEI backbone that was (were) involved in the formation of the adduct with the penetrant. In fact, there were several possible candidates, such as the imide carbonyls, the ether oxygens and, to a lesser extent, the aromatic rings. The analysis was performed by detecting the perturbation brought about by the probe to the spectrum of the substrate in terms of peak shifts and/or band-shape distortion, effects that were subsequently interpreted in terms of geometry and electron-density distribution of the molecular aggregate. The reversibility of the observed effects was also assessed, i.e., the obtainment of the unperturbed spectrum when the probe was fully desorbed. Measurements of this kind require films in the thickness range of 1.0–3.0 μm , in order to maintain the whole spectrum within the range of absorbance linearity. In the present case, these films were prepared ad hoc via a spin-coating process. Since the interaction was weak, the effects were expected to be very subtle; in these circumstances, difference spectroscopy was demonstrated to be a viable approach [46]. In Figure 8, the difference spectra in the frequency range 1820–1660 cm^{-1} are reported, obtained by subtracting the spectrum of the fully dried sample from the spectra of the polymer sample equilibrated with gaseous CO_2 at a pressure of 150 Torr and at the different temperatures. It is explicitly noted that the reference and the sample spectra to be subtracted were collected at the same temperature to avoid

any spurious perturbation of the vibrational response. Lowering the temperature is expected to narrow the peaks while increasing the separation among the components, which should enhance the shift effect. An increase in the number of interacting CO₂ molecules is also possible at lower temperatures, as a consequence of the reduced kinetic energy of the probe.

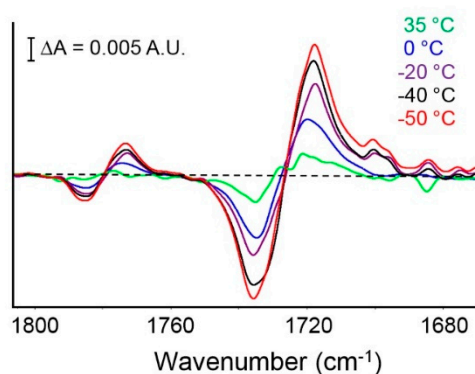


Figure 8. Difference spectra in the PEI carbonyl range. The subtraction involves the film equilibrated at the indicated temperatures as a sample spectrum and the fully dried sample as a reference. Both spectra were collected at the indicated temperatures. Equilibrium sorption measurements were performed at 150 Torr.

The difference spectra in Figure 8 display the typical first-derivative features associated with red-shifts, that is, a negative lobe preceding the positive. Thus, a lowering of the peak frequency was produced in the CO₂-containing samples. The effect was evident for both peaks occurring in the 1800–1680 cm⁻¹ interval, according to the nature of the corresponding vibrational modes, i.e., the in-phase, $\nu_{ip}(C=O)$, and out-of-phase stretching, $\nu_{oop}(C=O)$, of the imide carbonyls. The two-lobe profiles were symmetric, i.e., the positive and the negative components had comparable intensities and grew progressively as the temperature decreased. Furthermore, the effect was fully reversible, as demonstrated by comparing the reference spectrum with that of the sample equilibrated at $p = 150$ Torr and subsequently desorbed. These results confirm that the observed shifts, albeit very subtle (maximum shift of the main carbonyl component = 0.25 cm⁻¹), actually originated from the probe/substrate interactions and that these interactions were weak. For comparison, we recall that the red-shift caused by the interaction of the same carbonyl groups with water molecules (H-bonding) amounted to 0.8 cm⁻¹ [46]. All difference spectra were featureless below 1250 cm⁻¹. The absorbance spectrum of PEI displays two intense bands at 1238 and 1215 cm⁻¹, involving significant contributions from the C–O–C stretching modes [46]. The fact that these bands (as well as aromatic peaks) remained unaffected indicates that both the ether oxygens and the aromatic rings did not “see” the presence of the CO₂ molecules. The effects discussed above clarify the interaction mechanism: the imide carbonyls were selectively involved in a way that produced a lowering of the C=O force constant. The carbon atom of the carbon dioxide molecule, which brought a partial positive charge as a consequence of the two oxygens to which it was bound, formed a weak Lewis acid/Lewis base interaction with the imide carbonyls, as schematically represented in Figure 9. The above conclusions are in full agreement with the 2D-COS analysis.

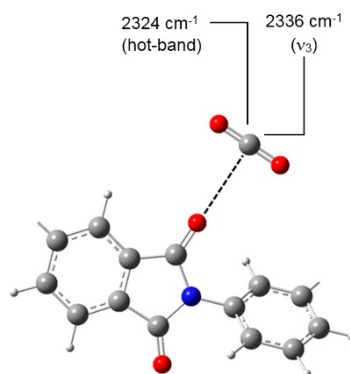


Figure 9. Schematic representation of the $\text{CO}_2/\text{C}=\text{O}$ interaction.

4.1.2. Modeling Sorption Thermodynamics

The FTIR analysis presented in the previous section indicates that carbon dioxide molecules absorbed within PEI tended to establish weak Lewis acid/Lewis base interactions with carbonyls along the polymer backbone. The interactional energy was close to a mean field value; hence, for the sake of a macroscopic thermodynamics description of the system, it was pointless to introduce distinct specific interaction terms in the model (as for the NETGP-NRHB model). Based on these premises, the NELF approach (see Appendix A, for relevant equations) was used, which provided a good interpretation of gravimetric sorption isotherms. In Figure 10, the experimental gravimetric sorption isotherms, along with the curves obtained by a concurrent fitting of the data with the NELF model at three temperatures (18, 27, and 35 °C), are reported. Only one fitting parameter, i.e., the Sanchez–Lacombe binary interaction parameter, χ_{12} (see Appendix A, for its definition), was used. A value of $\chi_{12} = 0.0313 \pm 0.003$ was estimated, thus pointing to a limited deviation from the geometric mixing rule for characteristic pressure (see Equation (A24)). The scaling parameters for the SL EoS of pure PEI were calculated by fitting pressure, volume, and temperature (PVT) data available from a previous investigation [20] with the SL-EoS model, while those of pure CO_2 were taken from Reference [26]. The (non-equilibrium) density values of neat PEI (i.e., $\rho_{2,\infty}$ as defined in Appendix A) at each temperature (assumed here to be time-independent) used in the model were taken from the literature [20]. All parameters are reported in Tables 1 and 2.

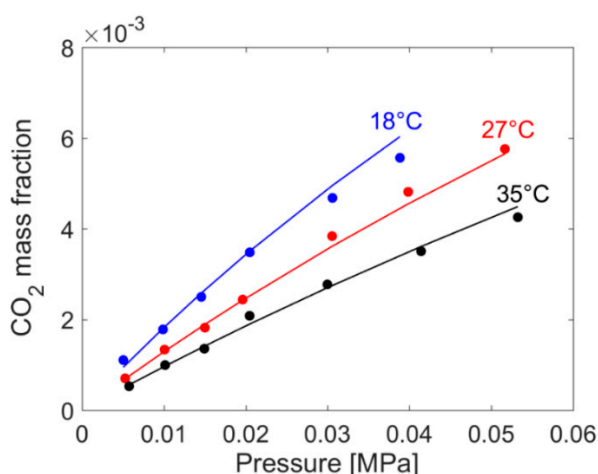


Figure 10. Experimental gravimetric sorption isotherms of CO_2 in PEI at 18, 27, and 35 °C. Continuous lines represent the results of concurrent data fitting performed with the non-equilibrium lattice fluid (NELF) model.

Table 1. Non-equilibrium polyetherimide (PEI) density [47].

Temperature (°C)	Density (g/cm ³)
18	1.2700 ± 0.0006
27	1.2680 ± 0.0006
30	1.2673 ± 0.0006
35	1.2663 ± 0.0006
45	1.2641 ± 0.0006
60	1.2610 ± 0.0006
70	1.2589 ± 0.0006

Table 2. Scaling parameters of Sanchez–Lacombe equation of state (EoS) for PEI and CO₂ [26,47].

Substance	T* (K)	P* (MPa)	ρ* (g/cm ³)
PEI	893	545	1.354
CO ₂	300	630	1.515

4.2. PEI–H₂O System

4.2.1. FTIR Analysis: Absorbance, Difference, and Two-Dimensional Correlation Spectra

For the analysis of water absorbed in PEI, we considered the normal modes of the water molecule in the $\nu(\text{OH})$ frequency range (3800–3200 cm⁻¹). Other regions of potential interest for the spectroscopic analysis were not available for the case at hand due the exceedingly low intensity of the signals. This system was discussed in a recent publication [46], and we present here the most relevant results.

In Figure 11A, the difference spectra in the OH stretching region ($\nu(\text{OH})$) are reported for the sample equilibrated with water vapor at different p/p_0 values. The band was representative of sorbed water and exhibited a profile with two maxima at 3655 and 3562 cm⁻¹. The well-resolved multicomponent band-shape clearly indicated the occurrences of different water species in contrast to the situation observed in the case of CO₂, where a single component pattern was detected.

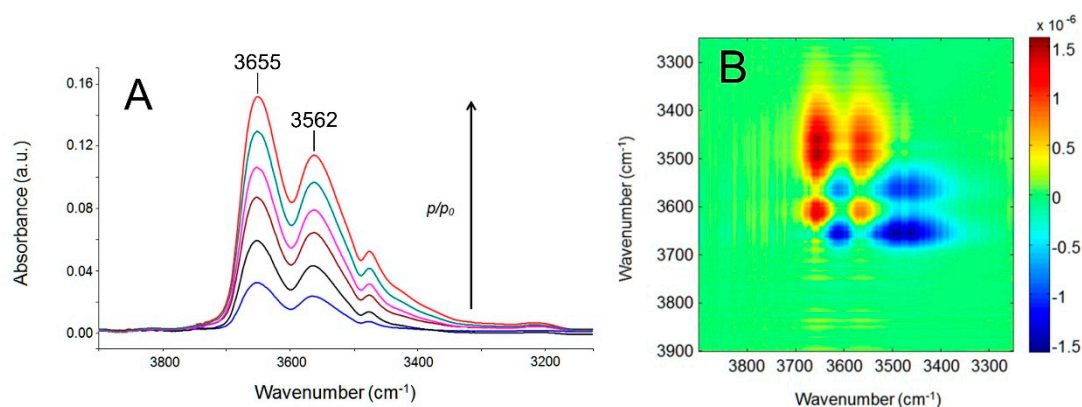


Figure 11. (A) The $\nu(\text{OH})$ band of H₂O sorbed in PEI after sorption equilibrium at different p/p_0 at 30 °C. (B) Asynchronous spectrum obtained from the time-resolved spectra collected during the sorption experiment performed at $p/p_0 = 0.6$ and 30 °C.

To improve the resolution and to deepen the spectral interpretation, 2D-COS was also carried out in this case; the time-resolved spectra collected during a water sorption experiment performed at a $p/p_0 = 0.6$ were used for this purpose. The resulting asynchronous spectrum is reported in Figure 11B. The rich pattern contrasts with the featureless map detected for the CO₂–PEI system (compare Figure 11B with Figure 7A), thus confirming that asynchronous 2D-COS spectra are a powerful and sensitive tool to highlight complex molecular interaction scenarios. In particular, in the case of the H₂O–PEI system, it emerged that there existed two couples of signals, suggesting the presence of two distinct

water species. In detail, the two sharp peaks at $3655\text{--}3562\text{ cm}^{-1}$ were assigned to the asymmetric and the symmetric stretching modes (ν_{as} and ν_{s}), respectively, of isolated water molecules interacting via H-bonding with the PEI backbone (cross-associated or first-shell water molecules). The second doublet at $3611\text{--}3486\text{ cm}^{-1}$ was related to water molecules self-interacting with the first shell species (self-associated or second-shell water molecules).

To identify the active sites of polymer backbone involved in the specific interaction with first-shell water molecules, an analysis was performed on thin samples (thickness in the range $1.0\text{--}3.0\text{ }\mu\text{m}$). The red-shift of the $\nu_{\text{ip}}(\text{C}=\text{O})$ and $\nu_{\text{oop}}(\text{C}=\text{O})$ modes demonstrated the involvement of the imide carbonyls as proton acceptors in H-bonding. The peaks of the aryl ether groups remained unperturbed, which demonstrated that their interaction with water was negligible, if present. In addition, it was found that the largely prevalent stoichiometry of the first-shell adduct was 2:1, i.e., a single water molecule bridged two carbonyls: $\text{--C}=\text{O}\text{--H}\text{--O}\text{--H}\text{--O}=\text{C}\text{--}$. The two water species identified spectroscopically are schematically represented in Figure 12, where the peak frequencies they produced are also indicated.

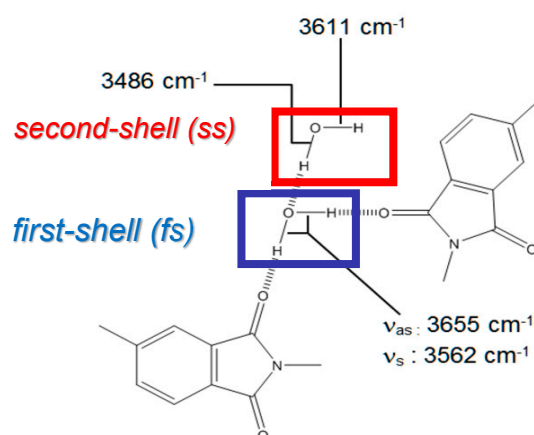


Figure 12. Schematic representation of the water species identified by the spectroscopic analysis.

Molecular dynamics (MD) calculations performed on this system [46] indicated that, at least in the low-to-intermediate relative pressure range of water vapor, these bridges formed by first-shell water were intramolecular, that is, formed by interacting with two contiguous carbonyl groups present on the same macromolecule. In Figure 13, a snapshot of an MD calculation is reported, showing the typical conformation of first-shell water molecules.

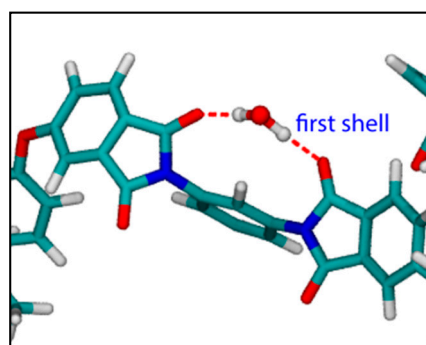


Figure 13. Snapshot of a typical first-shell (fs) configuration with an interacting water molecule bridging two consecutive carbonyl oxygens on the same PEI chain via hydrogen bonds.

Performing a quantitative analysis of the difference spectra of water, based on the information available from gravimetric measurements at different relative humidity, it was possible to obtain a quantitative estimation of the amount of the two water species identified spectroscopically. Details on the calculation procedure are reported in a previous publication [46].

4.2.2. Modeling Sorption Thermodynamics

In view of the significant HB interactions characterizing the PEI–H₂O system, the interpretation of sorption thermodynamics of water in glassy PEI was approached using the NETGP-NRHB model (see Appendix A for the relevant equations). Information gathered from the vibrational spectroscopy investigation, illustrated in Section 4.2.1, was exploited to tailor the H-bonding interaction contributions in the NETGP-NRHB model. In fact, only one proton acceptor was assumed to be present on the polymer backbone (i.e., the carbonyl of the imide group) and water molecules were assumed to be involved both in cross and self HB interactions. Moreover, the presence of two proton donors and two proton acceptors was assumed for each water molecule.

Also in this case, as for the PEI–CO₂ system, the non-equilibrium density of the polymer, at the different temperatures, was assumed to be time-independent and its value was taken to be equal to that of pure PEI. These density values, the values of the NRHB EoS scaling parameters for pure PEI and pure water, and the values of the self HB parameters for pure water were retrieved from the literature [20,75] and are reported in Tables 1 and 3. Experimental gravimetric water sorption isotherms in PEI were available at four temperatures (30, 45, 60, and 70 °C) [47]. For the meanings of scaling and HB interaction parameters appearing in Table 3, the reader is referred to Appendix A.

Table 3. Non-random lattice fluid hydrogen bonding (NRHB) scaling parameters and hydrogen-bonding (HB) interaction parameter for pure PEI and H₂O [20,75]. The meanings of symbols can be found in Appendix A.

Substance	ε_s^* (J/mol)	ε_h^* (J/(molK))	$v_{sp,0}^*$ (cm ³ /g)	E_{11}^{0w} (J/mol)	S_{11}^{0w} (J/(molK))	s	V_{11}^{0w} (cm ³ /mol)
PEI	6775 ± 250	5.503 ± 0.15	0.7228 ± 0.08	-	-	0.743 ^a	-
H ₂ O ^b	5336.5	-6.506	0.9703	-16,100	-14.7	0.861	0

^a Calculated using UNIFAC group contribution calculation scheme [76,77]. ^b No confidence intervals were provided for water parameters in Reference [75].

Concurrent fitting of the four experimental gravimetric isotherms was performed using the NETGP-NRHB model, and the results are shown in Figure 14. The internal energy of formation of water–polymer cross HB, E_{12}^{0wp} , the entropy of formation of water–polymer cross HB, S_{12}^{0wp} , and the mean field binary interaction parameter, K_{12} , were used as fitting parameters (their meanings are discussed in Appendix A). In accordance with the previous relevant literature [65], the volume of formation of water–polymer cross HB, V_{12}^{0wp} , was taken to be equal to zero. In Table 4, the values of the model parameters as determined by a best fitting procedure along with their 95% confidence intervals are reported, determined using the Jacobian method implemented in the *nlinfit* and *nlparci* routines of the Matlab[®] software. As evident in Figure 14, the model provided a very good fitting of the experimental sorption isotherms. Calculations performed to carry out isotherm data fitting using the NETGP-NRHB model also provided a prediction for the amount of self HB (i.e., 1–1, involving only water molecules) and of cross HB (i.e., 1–2, between water molecules and carbonyl groups of PEI) interactions established in the PEI–water mixture equilibrated with water vapor at the different p/p_0 investigated. In particular, calculations provided the number of moles of HB self-interactions (1–1) and of moles of HB cross-interactions (1–2) per gram of amorphous PEI, indicated as n_{11}/m_2 and n_{12}/m_2 , respectively. These values predicted using the NETGP-NRHB model, at a temperature of 30 °C, are compared in Figure 15 with the results obtained from FTIR spectroscopy and with the outcomes of MD simulations [46]. The agreement is satisfactory in the whole range of water concentrations.

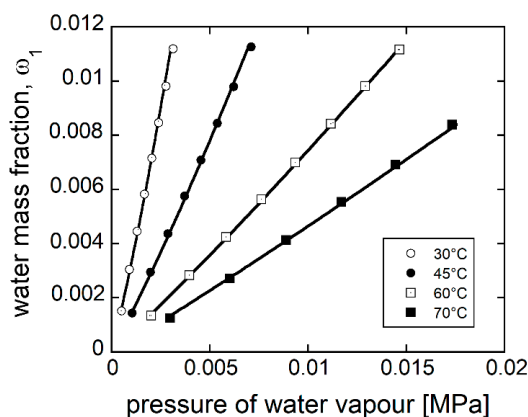


Figure 14. Experimental gravimetric sorption isotherms of H₂O in PEI at 30, 45, 60, and 70 °C. Dotted lines represent the results of concurrent data fitting performed with the non-equilibrium thermodynamics for glassy polymers/non-random lattice fluid hydrogen bonding (NETGP-NRHB) model.

Table 4. Non-equilibrium thermodynamics for glassy polymers (NETGP)-NRHB fitting parameters for PEI–water mixture (note that the value of V_{12}^{0wp} was set at 0 according to Reference [24]).

k_{12}	E_{12}^{0wp} (J/mol)	S_{12}^{0wp} (J/(mol·K))	V_{12}^{0wp} (cm ³ /mol)
0.121 ± 0.005	$-13,264 \pm 200$	-6.107 ± 0.100	0

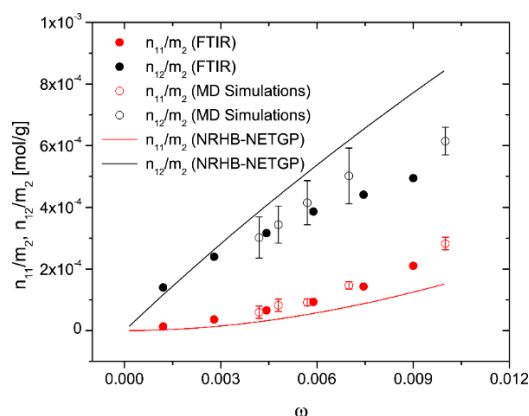


Figure 15. Comparison of the predictions of the NETGP-NRHB model for the number of self and cross HBs in the PEI–H₂O system at 30 °C with the outcomes from FTIR spectroscopy and of molecular dynamics (MD) simulations.

4.3. PEI–CH₃OH System

FTIR Analysis: Absorbance, Difference, and Two-Dimensional Correlation Spectra

For the methanol–PEI system at 30 °C, the $\nu(\text{OH})$ band-shape (3650–3200 cm⁻¹ range) was simpler than for water–PEI (compare Figures 16A and 11A) [47,48]. A single maximum was observed at 3575 cm⁻¹, superimposed to a broader component at lower frequencies. The occurrence of two signals only was confirmed by the asynchronous map (Figure 16B) displaying a single cross-correlation centered at 3441–3575 cm⁻¹. The other features appearing in the map were relative to the correlations with the $\nu(\text{CH})$ signals and were not relevant for the molecular interaction analysis. Perturbation analysis of the PEI spectrum indicated that the carbonyl groups of the polyimide acted as proton acceptors in the H-bonding interaction with methanol, while the $\nu(\text{C–O–C})$ band was unperturbed in the presence of methanol, thus indicating that the involvement of ether linkages in H-bonding with the penetrant could be ruled out.

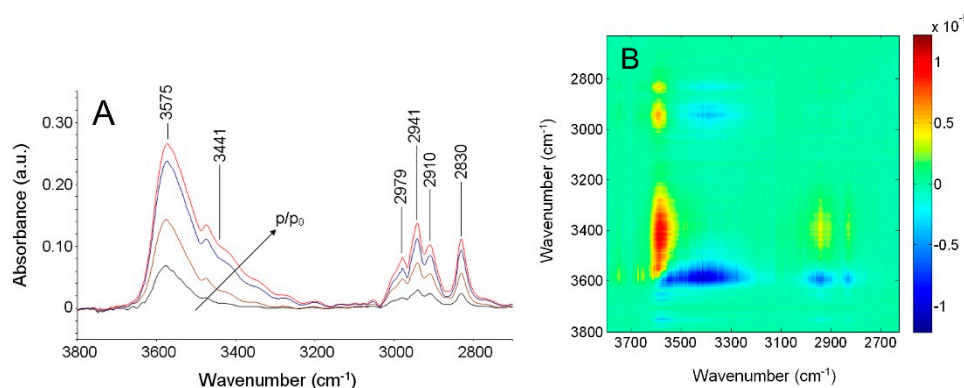


Figure 16. (A) The $\nu(\text{OH})$ ($3650\text{--}3200\text{ cm}^{-1}$ range) and $\nu(\text{OH})$ ($3650\text{--}3200\text{ cm}^{-1}$ range) of CH_3OH sorbed in PEI after sorption equilibrium at different p/p_0 at $30\text{ }^\circ\text{C}$. (B) Asynchronous spectrum obtained from the time-resolved spectra collected during the sorption experiment performed at $p/p_0 = 0.6$ and $30\text{ }^\circ\text{C}$.

In the light of all the experimental evidence, the peak at 3575 cm^{-1} was assigned to the OH group of methanol directly to the imide carbonyl, which represents the first-shell layer of the sorbed penetrant. The peak at 3441 cm^{-1} was due to self-associated methanol molecules (dimers), and in particular to the OH group bonded to oxygen of the first-shell species. A schematic representation the H-bonding aggregates established in the CH_3OH –PEI system is depicted in Figure 17.

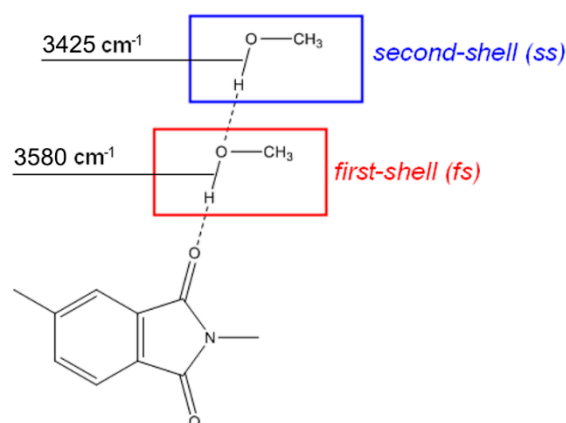


Figure 17. Schematic representation of the methanol species identified by the spectroscopic analysis.

As for the case of water, it was possible to quantify the amount of each of the two methanol species, as a function of the relative pressure of the methanol vapor phase at sorption equilibrium, by combining the gravimetric sorption isotherm, reported in Figure 18, with the results available from vibrational spectroscopy (see Figure 19) [47,48].

It was noted that, in the investigated range of relative pressure, the concentration of first-shell methanol, C_{fs} , was significantly higher than that of second-shell methanol, C_{ss} , thus indicating that, in this range, the monomer (i.e., a single molecule of methanol linked via HB to a carbonyl group), whose concentration was equal to $C_{fs} - C_{ss}$, was the largely prevailing species while self-associated aggregates were in a smaller amount and were likely to be dimers.

Fitting of the sorption isotherm was attempted both with the NELF and the NETGP-NRHB models assuming a time-independent value of polymer density, but the results were not satisfactory, likely due to a non-negligible structural evolution of PEI during methanol sorption. Since information on the actual value of polymer density was not available, we were not able to properly interpret the results with the illustrated class of lattice fluid models.

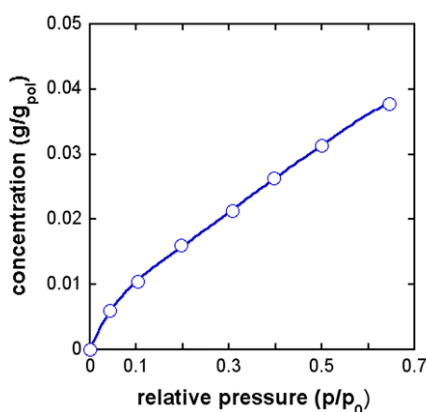


Figure 18. Experimental gravimetric sorption isotherms of CH_3OH in PEI at $30\text{ }^\circ\text{C}$. The continuous line does not represent any model and is intended to guide the eye.

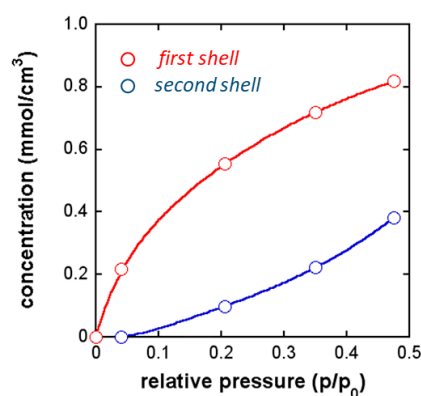


Figure 19. Amount of first- and second-shell methanol in PEI at equilibrium with pure methanol vapor phase at different relative pressures and at $30\text{ }^\circ\text{C}$. Continuous lines do not represent any model and are intended to guide the eye.

5. Conclusions

A molecular insight into sorption thermodynamics of low-molecular-weight penetrants in a glassy PEI was gained in the case of three penetrants with different interactive characteristics. To this aim, gravimetric analysis and FTIR spectroscopy were combined with macroscopic thermodynamics modeling.

For the case of sorption of carbon dioxide and water, non-equilibrium compressible lattice fluid theories were successfully used to interpret the experimental results. For the analysis of sorption data of carbon dioxide, an extension to non-equilibrium glassy polymers of the equilibrium Sanchez–Lacombe theory was adopted—the so-called NELF model. Conversely, for the case of water sorption, data were interpreted using an extension to non-equilibrium glassy polymers of the original NRHB approach—the so-called NETGP-NRHB model—to cope with specific H-bonding interactions occurring in the PEI– H_2O system.

In both cases, information gathered from vibrational spectroscopy was useful to choose the proper model and to tailor its structure. In fact, in the case of carbon dioxide, in view of the weak interactions established with groups present on the polymer backbone, the NELF approach, which does not explicitly account for specific interactions, was well suited to describe sorption thermodynamics. On the other hand, in the case of water, FTIR spectroscopy revealed the occurrence of two water species, one self-interacting via H-bonding and the other cross-interacting with carbonyl groups of PEI. This identification of the interactions to be accounted for in the sorption thermodynamics interpretation allowed us to tailor the structure of the H-bonding terms in the NETGP-NRHB model. In this case, FTIR analysis also provided quantitative information on self and cross HB interactions

established within the system, which was in remarkably close agreement with predictions of the adopted theoretical approach.

In the case of methanol, we were not able to identify a suitable theoretical approach, likely due to the effect of the penetrant on the density of the polymer substrate in the time frame of the experiments. In this case, we limited ourselves to the spectroscopic identification of the molecular aggregates and the population analysis.

Author Contributions: Conceptualization, G.M. and P.M.; methodology, G.S. and P.L.M.; software, G.S.; formal analysis, G.M. and P.M.; investigation, G.S. and P.L.M.; data curation, G.S. and P.L.M.; writing—original draft preparation, G.M. and P.M.; writing—review and editing, G.M. and P.M.

Funding: This research received no external funding.

Conflicts of Interest: The authors declare no conflicts of interest.

Appendix A

A.1. The Equilibrium NRHB Model

The NRHB model [2,24,25] is an equation of state model for fluids used to describe the equilibrium thermodynamics of pure components and mixtures. The model is based on a non-random compressible lattice characterized by the presence of empty sites and accounting for hydrogen-bonding interactions. Each molecule of type i occupies r_i sites (or cells) of the lattice; this value is independent of the composition of the system. The total number of molecules in a system, N , is arranged in a lattice consisting of N_r sites, including N_0 empty sites. The lattice is characterized by a coordination number, z , that is generally assumed to be equal to 10. The system is made of N_1 molecules of type 1, N_2 molecules of type 2, and N_t molecules of type t , and is endowed with hydrogen-bonding specific interactions involving m types of proton donors and n types of proton acceptors. The model is based on a Gibbs partition function, Ψ , for the system, characterized by a tractable mathematical structure based on the assumption that the canonical partition function, Q , can be factorized in two contributions—one related to intermolecular interactions, apart from specific ones, and one associated to specific interactions. This corresponds to the decoupling of physical (van der Waals) and specific (hydrogen bonding) interactions. The canonical partition function is expressed as

$$Q = Q_P(T, N_0, N_1, N_2, \dots, N_t) \cdot Q_H(T, N_0, N_1, N_2, \dots, N_t), \quad (\text{A1})$$

where the subscript P stands for “physical” and the subscript H stands for “hydrogen bonding”.

The physical contribution to the canonical partition function is, in turn, expressed as

$$Q_P(T, N_0, N_1, N_2, \dots, N_t) = \sum_{\underline{N}_{ij}} Q_P(T, N_0, N_1, N_2, \dots, N_t, \underline{N}_{ij}), \quad (\text{A2})$$

where \underline{N}_{ij} represents a vector of variables, whose generic N_{ij} component represents the number of lattice fluid contacts between a segment of a molecule of type i and a segment of a molecule of type j , with i ranging from 0 to t and $j \geq i$. It is worth noting that not all the possible N_{ij} variables are present in this vector, since they are not all independent of each other. In fact, the following material balance equation holds:

$$2N_{ii} + \sum_{i \neq j} N_{ij} = N_i z q_i, \quad (\text{A3})$$

where $z q_i$ is the number of external lattice contacts per molecule for component i . As a consequence, the independent subset of variables is that made of N_{ij} with i ranging from 0 to t and $j > i$.

The hydrogen-bonding contribution to the canonical partition function is expressed as

$$Q_H(T, N_0, N_1, N_2, \dots, N_t) = \sum_{\underline{N}_{\alpha\beta}^{HB}} Q_H(T, N_0, N_1, N_2, \dots, N_t, \underline{N}_{\alpha\beta}^H), \tag{A4}$$

where $\underline{N}_{\alpha\beta}^H$ represents a vector of variables, whose generic $N_{\alpha\beta}^H$ component represents the total number of hydrogen-bonding interactions between proton donor groups of type α and proton acceptor groups of type β .

The Gibbs partition function, Ψ , can be then calculated from Q as follows:

$$\Psi(T, P, N_1, N_2, \dots, N_t) = \sum_{N_0=0}^{\infty} \left[Q_P(T, N_0, N_1, N_2, \dots, N_t) \cdot Q_H(T, N_0, N_1, N_2, \dots, N_t) \cdot \exp\left(-\frac{PV}{kT}\right) \right] \tag{A5}$$

where P and V are the pressure and the volume, respectively, of the mixture. It is noted that in the NRHB model, the “physical” canonical partition function, Q_P , is in turn factorized in two terms: a random term, Q_{PR} , and a non-random correction, Q_{PNR} , which accounts for the non-random distribution of contacts. Full details can be found in Reference [25].

The Gibbs energy can be then readily obtained as

$$G = -kT \ln[\Psi(T, P, N_1, N_2, \dots, N_t)] \tag{A6}$$

According to a standard procedure of statistical thermodynamics, the sum in Equation (A5) can be approximated by its maximum term. This is mathematically equivalent to equating G to the logarithm of the generic term of the Gibbs partition function and finding its minimum with respect to the variables \underline{N}_{ij} , $\underline{N}_{\alpha\beta}^H$ and N_0 .

This minimization procedures result in the following expressions [24,25]:

$$\frac{\Gamma_{ij}^2}{\Gamma_{ii} \Gamma_{jj}} = \exp\left(\frac{\Delta\epsilon_{ij}}{RT}\right); \tag{A7a}$$

$$\frac{v_{\alpha\beta}}{v_{\alpha 0} v_{0\beta}} = \tilde{\rho} \exp\left(\frac{-G_{\alpha\beta}^H}{RT}\right); \tag{A7b}$$

$$\tilde{P} + \tilde{T} \left[\ln(1 - \tilde{\rho}) - \tilde{\rho} \left(\sum_{i=1}^t \varphi_i \frac{l_i}{r_i} - \nu_H \right) - \frac{z}{2} \ln\left(1 - \tilde{\rho} + \frac{q}{r} \tilde{\rho}\right) + \frac{z}{2} \ln \Gamma_{00} \right] = 0. \tag{A7c}$$

In Equation (A7a), the Γ_{ij} 's are non-random factors defined as N_{ij}/N_{ij}^0 , where N_{ij}^0 represents the number of lattice fluid contacts between a segment of a species of type i and a segment of a species of type j in the case of random arrangement of contacts in the lattice and $\Delta\epsilon_{ij}$ is defined by the expression

$$\Delta\epsilon_{ij} = \epsilon_i + \epsilon_j - 2(1 - k_{ij}) \sqrt{\epsilon_i \epsilon_j}, \tag{A8}$$

where ϵ_i is the interaction energy per i - i contact within the lattice and k_{ij} is the mean field binary interaction parameter measuring the deviation from geometric mixing rule for characteristic energies.

In Equation (A7b), $v_{\alpha\beta}$ represents the average number per molecular segment of hydrogen bonding established between a proton donor of type α and a proton acceptor of type β ; $v_{\alpha 0}$ and $v_{0\beta}$ are the average number of unbonded proton donors of type α and the average number of unbonded proton acceptors of type β , respectively, per molecular segment; and $G_{\alpha\beta}^H$ is the molar Gibbs energy of formation of hydrogen bonding between proton donor group of type α and proton acceptor group of type β . The term $G_{\alpha\beta}^H$ is equal to $E_{\alpha\beta}^H - TS_{\alpha\beta}^H + PV_{\alpha\beta}^H$, where $E_{\alpha\beta}^H$, $S_{\alpha\beta}^H$, and $V_{\alpha\beta}^H$ are the molar internal energy, entropy, and volume of formation of hydrogen bonding, respectively, between proton donor

group of type α and proton acceptor group of type β . The value of $V_{\alpha\beta}^H$ is generally taken as being equal to zero [65].

In Equation (A7c), representing the equation of state of the mixture, \tilde{P} , \tilde{T} , and $\tilde{\rho}$ are the scaled pressure, the scaled temperature, and scaled density of the mixture, respectively; φ_i is the “close-packed” volumetric fraction of component i , zq is the averaged number of external lattice contacts per molecule in the mixture, r is the average number of cells occupied per molecule in the mixture, ν_H is the total number of hydrogen bonds per -mer in the mixture, and l_j is a parameter that can be calculated using the following expression [25]:

$$l_j = \frac{z}{2}(r_j - q_j) - (r_j - 1). \tag{A9}$$

The resulting general expression of the chemical potential for the component i in the polymer mixture is given as follows [25]:

$$\begin{aligned} \frac{\mu_{i,POL}}{RT} = \ln \frac{\varphi_i}{\delta_i r_i} &- r_i \sum_{j=1}^t \frac{\varphi_j l_j}{r_j} + \ln \tilde{\rho} + r_i(\tilde{v} - 1)\ln(1 - \tilde{\rho}) \\ &- \frac{z}{2} r_i \left[\tilde{v} - 1 + \frac{q_i}{r_i} \right] \ln \left[1 - \tilde{\rho} + \frac{q}{r} \tilde{\rho} \right] + \frac{z q_i}{2} \left[\ln \Gamma_{ii} + \frac{r_i}{q_i} (\tilde{v} - 1) \ln \Gamma_{00} \right] \\ &+ r_i \frac{\tilde{P} \tilde{v}}{\tilde{T}} - \frac{q_i}{\tilde{T}_i} + \frac{\mu_{i,POL}^H}{RT}, \end{aligned} \tag{A10}$$

where the hydrogen-bonding contribution to the penetrant chemical potential, $\mu_{i,POL}^H$, is given as follows [9]:

$$\frac{\mu_{i,POL}^H}{RT} = r_i \nu_H - \sum_{\alpha=1}^m d_{\alpha}^i \ln \left(\frac{v_d^{\alpha}}{v_{\alpha 0}} \right) - \sum_{\beta=1}^n a_{\beta}^i \ln \left(\frac{v_a^{\beta}}{v_{0\beta}} \right). \tag{A11}$$

In the previous expressions $\tilde{v} = 1/\tilde{\rho}$, δ_i is the number of configurations available to a molecule of component i in the “close-packed” state and is a characteristic quantity for the penetrant that accounts for the flexibility and the symmetry of the molecule (it cancels out in all equilibrium calculations of interest here), \tilde{T}_i is the scaled temperature of pure component i , d_{α}^i is the number of proton donors of type α on the molecule of type i , a_{β}^i is the number of proton acceptors of type β on the molecule of type i , and v_d^{α} and v_a^{β} are the total number of proton donors of type α and the average number of proton acceptors of type β , respectively, per -mer in the mixture.

The expression of equilibrium chemical potential for component i in the mixture can be obtained by coupling Equations (A7a)–(A7c) with Equation (A10). Phase equilibrium between a gas mixture and a polymer mixture is dictated by the equivalence of the equilibrium chemical potentials of each component in the two phases. In the case of penetrant sorption in a fluid or solid polymer, it is generally assumed that no polymer is present in the gaseous phase, and that the equilibrium is dictated only by the equivalence of chemical potentials of penetrants in the two phases.

The physical canonical partition function carries three scaling parameters for each component: (a) the enthalpic, ε_h^* , and the entropic, ε_s , contribution to the mean field interaction energy per mole of segment, and (b) $v_{sp,0}^*$ that is, the “close-packed” specific volume of the pure component at a reference temperature (298.15 K). For the case of a pure component i , the mean interaction energy per mole of segment, ε_{ii}^* , is expressed as

$$\varepsilon_{ii}^* = \varepsilon_h^* + (T - 298.15)\varepsilon_s^*. \tag{A12}$$

The so-called “close-packed” volume of a component (i.e., when no empty sites are present), can be calculated using the following equation (where v_{sp}^* is expressed in $\text{cm}^3 \cdot \text{g}^{-1}$):

$$v_{sp}^* = v_{sp,0}^* + (T - 298.15)v_{sp,1}^* - 0.135 \times 10^{-3}P, \tag{A13}$$

where P is the pressure (in MPa). The pressure term in Equation (A13) is taken to be equal to zero for low-molecular-weight compounds. $v_{sp,1}^*$ is a parameter that takes the same value for a given homologous series, and its values can be retrieved from the literature [25].

The value of r_i is expressed as a function of the lattice cell volume, v^* , of the “close-packed” volume, v_{sp}^* and of the molecular weight MW_i of the component i .

$$r_i = \frac{MW_i v_{sp}^*}{v^*}, \quad (\text{A14})$$

where v^* is taken to be equal to $9.75 \text{ cm}^3 \cdot \text{mol}^{-1}$ for all fluids [25].

In the case of mixtures, proper mixing rules are introduced. Limiting the attention to binary mixtures, an average number of lattice cells occupied by a molecule in the mixture can be calculated as

$$r = \sum_{i=1}^2 r_i x_i, \quad (\text{A15})$$

where x_i represents the molar fraction of component i . The average lattice fluid intersegmental interaction energy per mole of average segment in the mixture is calculated as

$$\varepsilon^* = \sum_{i=1}^2 \sum_{j=1}^2 \theta_i \theta_j \varepsilon_{ij}^*, \quad (\text{A16a})$$

where

$$\varepsilon_{12}^* = (1 - k_{12}) \sqrt{\varepsilon_{11}^* \varepsilon_{22}^*}, \quad (\text{A16b})$$

and θ are the concentration-dependent surface fraction of component i in the mixture.

The reduced temperature of the mixture, \tilde{T} , the reduced temperature of component i , \tilde{T}_i , reduced pressure of the mixture, \tilde{P} , and reduced density of the mixture, $\tilde{\rho}$, can be expressed as

$$\tilde{T} = \frac{RT}{\varepsilon^*}; \quad \tilde{T}_i = \frac{RT}{\varepsilon_{ii}^*}; \quad \tilde{P} = \frac{v^* P}{\varepsilon^*}; \quad \tilde{\rho} = \frac{\rho}{\rho^*}, \quad (\text{A17})$$

where $\rho^* = \sum_{i=1}^2 \frac{x_i MW_i}{r v^*}$

A.2. Extension of Equilibrium Theories to Non-Equilibrium Glassy Polymers

Equilibrium models, such as the NRHB theory, are not suited to describing mixture thermodynamics of low-molecular-weight compounds and non-equilibrium glassy polymers. To extend equilibrium approaches to the case of non-equilibrium glassy polymers, Doghieri and Sarti elaborated a procedure denominated the “non-equilibrium thermodynamics for glassy polymers (NETGP)” approach [26,27,69], which is rooted in thermodynamics endowed with internal state variables. In this section, we illustrate briefly the particular case of the application of this extension procedure to the Sanchez–Lacombe model [54] for binary polymer–penetrant mixtures. This was the first example of application of the NETGP procedure [26,27] that was then applied to other equation of state equilibrium models. In the present context, we refer to this theory as the “non-equilibrium lattice fluid” (NELF) model. Throughout this section, the subscript 1 refers to the penetrant and the subscript 2 refers to the polymer. The Sanchez–Lacombe theory is significantly simpler than the NRHB approach and is based on a random compressible lattice fluid model which accounts neither for the non-randomicity of contacts nor for the establishment of specific interactions among the components of the mixture.

In their extension of the Sanchez–Lacombe model, Sarti and Doghieri assumed that, for the non-equilibrium glassy polymer/penetrant mixture, the thermodynamic state is identified by the following set of variables: temperature, pressure, number of moles of penetrant, n_1 , and density of

the polymer in the mixture, ρ_2 [26,27]. The density of the polymer is an order parameter that rules the departure from equilibrium and takes on the role of an internal state variable of the system, whose rate of change over time is itself a function of the state of the system.

$$\frac{d\rho_2}{dt} = f(T, P, n_1, \rho_2). \tag{A18}$$

In the implementation of this extension procedure, it is frequently feasible to assume $f(T, p, n_1, \rho_2) \cong 0$. In fact, in the case of polymer systems at temperatures well below their glass transition temperature, the density relaxation may occur on a time span much longer than that required to reach phase equilibrium, thus implying that ρ_2 is “frozen” at a roughly constant non-equilibrium value, referred to as $\rho_{2,\infty}$. This is legitimate for low concentrations of penetrant within the polymer. In such cases $\rho_{2,\infty}$ is taken as being equal to the starting value of dry polymer. We actually deal, in this case, with a pseudo phase equilibrium, in view of the non-equilibrium nature of the glassy polymer.

It can be demonstrated [27] that the phase pseudo-equilibrium between a pure penetrant gaseous phase and the “frozen” polymer–penetrant mixture is still dictated by the equivalence of chemical potentials. Assuming that no polymer is present in the gaseous phase, in a binary case, this condition applies only to the penetrant

$$\mu_{1,POL}(T, p, n_1^{PE}, \rho_{2,\infty}) = \mu_{1,GAS}(T, p), \tag{A19}$$

where $\mu_{1,POL}$ and $\mu_{1,GAS}$ are the penetrant chemical potential in the polymer phase and in the gaseous phase, respectively. In Equation (A19), $\mu_{1,GAS}$ is consistently provided by the Sanchez–Lacombe theory written for pure penetrant and is coupled with related equation of state expression. The symbol n_1^{PE} highlights that we refer to a pseudo-equilibrium polymer phase.

In Equation (A19), $\mu_{1,POL}$ is obtained by deriving the Gibbs energy as a function of the number of moles of penetrant.

$$\mu_{1,POL} = \left. \frac{\partial G}{\partial n_1} \right|_{T,p,\rho_2}. \tag{A20}$$

The expression for G is provided by an expression similar to Equation (6) where the partition function Ψ is evaluated, using the expression provided by Sanchez–Lacombe theory, considering only the generic term of the summation, evaluated at a single value of ρ_2 . Actually, a change of variable is introduced, expressing this generic term as a function of ρ_2 using the following relationship that relates ρ_2 to N_0 :

$$\rho_2 = \frac{m_2}{V} = \frac{m_2}{rNv^* + N_0v^*}, \tag{A21}$$

where m_2 is the mass of polymer in the polymer–penetrant mixture (that is fixed). In performing the derivative in Equation (A20), the generic term for G is evaluated at $\rho_2 = \rho_{2,\infty}$. By this procedure, Sarti et al. [26] obtained the following expression for $\mu_{1,POL}$ according to the NELF approach:

$$\frac{\mu_{1,POL}}{RT} = 1 + \ln(\tilde{\rho}\varphi_1) - \left[r_1^0 + \frac{(r_1 - r_1^0)}{\tilde{\rho}} \right] \ln(1 - \tilde{\rho}) - r_1 - \frac{\tilde{\rho}[r_1^0v_1^*(P_1^* + P^* - \varphi_2^2\Delta P^*)]}{RT}. \tag{A22}$$

It is worth noting that, unlike NRHB, in this model, the number of -mers occupied in the lattice by component i takes on different values for the component in the mixture (r_i , which is a function of concentration) and for the pure component (r_i^0). This last value is obtained by the scaling parameters of the model for the pure component i . P_i^* is the scaling parameter for the pressure in the Sanchez and Lacombe theory named “characteristic pressure” of pure component i , while P^* is obtained by a mixing rule as

$$P^* = \varphi_1P_1^* + \varphi_2P_2^* - \varphi_1\varphi_2 \Delta P^*, \tag{A23}$$

with

$$\Delta P^* = P_1^* + P_2^* - 2\chi_{12}\sqrt{P_1^*P_2^*}. \quad (\text{A24})$$

In Equation (A24), χ_{12} represents the Sanchez–Lacombe binary interaction parameter. It is worth noting that, unlike the case of equilibrium expression for chemical potential obtained by Sanchez–Lacombe theory, the expression (A22) for non-equilibrium chemical potential does not need to be coupled with the minimization condition for G as a function of N_0 .

In Equation (A22), we have

$$\tilde{\rho} = \frac{\rho_{2,\infty}}{\omega_2\rho^*}, \quad (\text{A25})$$

where ω_i is the mass fraction of component i and ρ is the “close-packed” density of the mixture, which is a function of concentration according to

$$\rho^* = -\frac{\rho_1^*\rho_2^*}{(-\omega_1\rho_2^* - \rho_1^* + \omega_1\rho_1^*)}, \quad (\text{A26})$$

where ρ_i^* is the scaling parameter for the density in the Sanchez–Lacombe theory for the component i .

The parameters of the NELF model are the binary interaction parameter, χ_{12} and the scaling parameters of each pure component, P_i^* , T_i^* , and ρ_i^* . T_i^* is the characteristic temperature of component i . The reduced pressure, temperature, and density of each component are consequently defined as

$$\tilde{P}_i = \frac{P}{P_i^*}; \quad \tilde{T}_i = \frac{T}{T_i^*}; \quad \tilde{\rho}_i = \frac{\rho}{\rho_i^*}. \quad (\text{A27})$$

For the mixture, the corresponding scaling parameters are P^* , T^* , and ρ^* , which can be obtained, by proper mixing rules, from the corresponding pure component quantities.

The binary interaction parameter can be retrieved by fitting sorption isotherms with the NELF model for chemical potential. Conversely, the pure component scaling parameters are generally obtained by fitting equilibrium PVT data in the case of polymers and liquid–vapor equilibrium data in the case of low-molecular-weight compounds. Obviously, the value of $\rho_{2,\infty}$ is also to be known and can be retrieved by standard methods for measuring the density of polymers (e.g., by helium picnometry).

A procedure similar to that applied by Sarti and Doghieri to develop the NELF approach was applied by our group to extend the NRHB model to the case of non-equilibrium glassy polymers [72], developing the so-called NETGP-NRHB model. The procedure is more complex since, in this case, the number of internal state variables is incremented. In fact, in addition to ρ_2 , there are also the variables $\underline{N}_{\alpha\beta}^H$ and the variables \underline{N}_{ij} with i ranging from 0 to t and $j > i$.

As already discussed, at equilibrium, the values of these variables are dictated by Gibbs energy minimization conditions. Conversely, in non-equilibrium conditions, the values of these variables are ruled by equations for their evolution kinetics that, in turn, are a function of the state of the system.

To simplify an otherwise complex matter, we assumed in developing the NETGP-NRHB approach that, in analogy to the NELF model, the evolution kinetics of ρ_2 is extremely slow. Conversely, we assumed that the evolution kinetics of all the other internal state variables is “instantaneous”. As a consequence, the values of variables $\underline{N}_{\alpha\beta}^H$ and \underline{N}_{ij} are those that the system would exhibit at equilibrium for the specific value of (non-equilibrium) $\rho_2 = \rho_{2,\infty}$ and for the current value of concentration at the system pressure and temperature. Consequently, in a binary system, the expression for chemical potential is the one obtained from

$$\mu_{1,POL} = \left. \frac{\partial G}{\partial n_1} \right|_{T, p, n_2, \rho_2, \underline{N}_{ij}, \underline{N}_{\alpha\beta}^H}, \quad (\text{A28})$$

where the values of $\underline{N}_{\alpha\beta}^H$ and \underline{N}_{ij} are obtained by the minimization conditions (A7a) and (A7b).

In Equation (A28), G is provided by Equation (6) where the partition function ψ is evaluated, using the expression provided by NRHB theory, considering only the generic term of the summation corresponding to $\rho_2 = \rho_{2,\infty}$ and to the values of $\underline{N}_{\alpha\beta}^H$ and \underline{N}_{ij} obtained by the minimization conditions.

Having made the hypothesis of “instantaneous equilibrium” for the variables $\underline{N}_{\alpha\beta}^H$ and \underline{N}_{ij} , the constitutive class for non-equilibrium system actually becomes the same as for NELF and, for a binary system, consists of the “external” variables T, P, n_1 , and n_2 and of the “internal” variable ρ_2 . We can then use the same arguments invoked for the NELF model to demonstrate that, at the phase pseudo-equilibrium between glassy polymer–penetrant phase and pure penetrant gaseous phase, the following equation holds:

$$\mu_{1,POL}(T, P, n_1^{PE}) = \left. \frac{\partial G}{\partial n_1} \right|_{T, p, n_2, \rho_2, \underline{N}_{ij}, \underline{N}_{\alpha\beta}^H} = \mu_{1,GAS}(T, P). \tag{A29}$$

In Equation (A29), $\mu_{1,GAS}$ is consistently provided by the equilibrium NRHB theory written for pure penetrant (see Section A.1) and is coupled with the related equation of state expression. The following expression was finally obtained [22] for the penetrant chemical potential in the polymer–penetrant mixture:

$$\begin{aligned} \frac{\mu_{1,POL}}{RT} = & \ln \frac{\varphi_1}{\delta_1 r_1} - r_1 \sum_{j=1}^2 \frac{\varphi_j^{Ij}}{r_j} + \ln \tilde{\rho} + r_1 (\tilde{v} - 1) \ln(1 - \tilde{\rho}) - \frac{z}{2} r_1 \left[\tilde{v} - 1 + \frac{q_1}{r_1} \right] \ln \left[1 - \tilde{\rho} + \frac{q}{r} \tilde{\rho} \right] \\ & + \frac{z q_1}{2} \left[\ln \Gamma_{11} + \frac{r_1}{q_1} (\tilde{v} - 1) \ln \Gamma_{00} \right] - \frac{q_1}{T_1} \\ & + \tilde{T} \left[\ln(1 - \tilde{\rho}) - \tilde{\rho} \left(\sum_{j=1}^2 \frac{\varphi_j^{Ij}}{r_j} \right) - \frac{z}{2} \ln(1 - \tilde{\rho} + \frac{q}{r} \tilde{\rho}) + \frac{z}{2} \ln \Gamma_{00} \right] \\ & \cdot \frac{r x_2 \left. \frac{\partial \tilde{v}}{\partial x_1} \right|_{P, T, \rho_2, \underline{N}_{ij}, \underline{N}_{\alpha\beta}^H}}{\tilde{T}} + r_1 v_H - \sum_i^m d_i^1 \ln \left(\frac{v_d^i}{v_{i0}} \right) - \sum_j^n a_j^1 \ln \left(\frac{v_a^j}{v_{0j}} \right) \\ & + v_H \left. \frac{\partial \ln \tilde{v}}{\partial x_1} \right|_{P, T, \rho_2, \underline{N}_{ij}, \underline{N}_{\alpha\beta}^H} x_2 r. \end{aligned} \tag{A30}$$

This expression, coupled with Equations (A7a) and (A7b), provides the values of non-equilibrium chemical potential of penetrant in the polymer–penetrant mixture, according to the NETGP-NRHB model.

The parameters of the NETGP-NRHB model are the NRHB EoS parameters for pure components, i.e., ε_h^* , ν_s , and $v_{sp,0}^*$, and the hydrogen bonding parameters, i.e., the $E_{\alpha\beta}^H$ and $S_{\alpha\beta}^H$ for each proton donor–proton acceptor couple. The values of EoS parameters and of the hydrogen-bonding parameters for pure component interactions (self hydrogen-bonding interactions) can be retrieved from equilibrium PVT data in the case of polymers and liquid–vapor equilibrium data in the case of penetrants. The hydrogen-bonding parameters for interactions between polymer and penetrant (cross hydrogen bonding interactions), as well as the binary interaction parameter, k_{12} , are retrieved from fitting of sorption isotherms with the NETGP-NRHB model. Regarding q_i , its value can be obtained as $q_i = s_i \times r_i$, where s_i is the surface-to-volume ratio for a molecule of component i and can be estimated using the UNIFAC group contribution model [77].

It is explicitly noted that, once fitting of the experimental sorption isotherms is carried out, the model calculations also provide a prediction for the values of the set of variables $\underline{N}_{\alpha\beta}^H$ and \underline{N}_{ij} for the mixture.

References

1. Kontogeorgis, G.M.; Folas, G.K. *Thermodynamic Models for Industrial Applications: From Classical and Advanced Mixing Rules to Association Theories*, 1st ed.; John Wiley & Sons, Ltd.: Chichester, UK, 2010; ISBN 978-0-470-69726-9.

2. Panayiotou, C.G.; Birdi, K.S. *Handbook of Surface and Colloid Chemistry*, 3rd ed.; CRC Press Taylor and Francis Group: New York, NY, USA, 2009.
3. Iwamoto, R.; Kusanagi, H. Hydration Structure and Mobility of the Water Contained in Poly(ethylene terephthalate). *J. Phys. Chem. A* **2015**, *119*, 2885–2894. [[CrossRef](#)] [[PubMed](#)]
4. Sammon, C.; Mura, C.; Yarwood, J.; Everall, N.; Swart, R.; Hodge, D. FTIR–ATR Studies of the Structure and Dynamics of Water Molecules in Polymeric Matrixes. A Comparison of PET and PVC. *J. Phys. Chem. B* **1998**, *102*, 3402–3411. [[CrossRef](#)]
5. Davis, E.M.; Elabd, Y.A. Water Clustering in Glassy Polymers. *J. Phys. Chem. B* **2013**, *117*, 10629–10640. [[CrossRef](#)] [[PubMed](#)]
6. Taylor, L.S.; Langkilde, F.W.; Zografi, G. Fourier transform Raman spectroscopic study of the interaction of water vapor with amorphous polymers. *J. Pharm. Sci.* **2001**, *90*, 888–901. [[CrossRef](#)] [[PubMed](#)]
7. De Angelis, M.G.; Sarti, G.C. Solubility of Gases and Liquids in Glassy Polymers. *Annu. Rev. Chem. Biomol.* **2011**, *2*, 97–120. [[CrossRef](#)] [[PubMed](#)]
8. Belova, N.A.; Safronov, A.P.; Yampolskii, Y.P. Inverse Gas Chromatography and the Thermodynamics of Sorption in Polymers. *Polym. Sci. Ser. A* **2012**, *54*, 859–873. [[CrossRef](#)]
9. Galizia, M.; Chi, W.S.; Smith, Z.P.; Merkel, T.C.; Baker, R.W.; Freeman, B.D. Polymers and Mixed Matrix Membranes for Gas and Vapor Separation: A Review and Prospective Opportunities. *Macromolecules* **2017**, *50*, 7809–7843. [[CrossRef](#)]
10. Glass, J.E. Adsorption characteristics of water-soluble polymers. I. Poly(vinyl alcohol) and poly(vinylpyrrolidone) at the aqueous-air interface. *J. Phys. Chem.* **1968**, *72*, 4450–4458. [[CrossRef](#)]
11. Zhao, Z.-J.; Wang, Q.; Zhang, L.; Wu, T. Structured Water and Water–Polymer Interactions in Hydrogels of Molecularly Imprinted Polymers. *J. Phys. Chem. B* **2008**, *112*, 7515–7521. [[CrossRef](#)]
12. Chiessi, E.; Cavalieri, F.; Paradossi, G. Water and Polymer Dynamics in Chemically Cross-Linked Hydrogels of Poly(vinyl alcohol): A Molecular Dynamics Simulation Study. *J. Phys. Chem. B* **2007**, *111*, 2820–2827. [[CrossRef](#)]
13. Eslami, H.; Müller-Plathe, F. Molecular Dynamics Simulation of Water Influence on Local Structure of Nanoconfined Polyamide-6,6. *J. Phys. Chem. B* **2011**, *115*, 9720–9731. [[CrossRef](#)] [[PubMed](#)]
14. Mensitieri, G.; Iannone, M. Modelling accelerated ageing in polymer composites. In *Ageing of Composites*, 1st ed.; Martin, R., Ed.; Woodhead Publishing, Ltd.: Cambridge, UK; CRC Press: Boca Raton, FL, USA, 2008; pp. 224–281. ISBN 9781845693527.
15. Li, D.; Yao, J.; Wang, H. Thin Films and Membranes with Hierarchical Porosity. In *Encyclopedia of Membrane Science and Technology*, 1st ed.; Hoek, E.M.V., Tarabara, V.V., Eds.; Wiley-Blackwell: Hoboken, NJ, USA, 2013; ISBN 978-0-470-90687-3.
16. Bernstein, R.; Kaufman, Y.; Freger, V. Membrane Characterization. In *Encyclopedia of Membrane Science and Technology*, 1st ed.; Hoek, E.M.V., Tarabara, V.V., Eds.; Wiley-Blackwell: Hoboken, NJ, USA, 2013; ISBN 978-0-470-90687-3.
17. Brunetti, A.; Barbieri, G.; Drioli, E. Gas Separation, Applications. In *Encyclopedia of Membrane Science and Technology*, 1st ed.; Hoek, E.M.V., Tarabara, V.V., Eds.; Wiley-Blackwell: Hoboken, NJ, USA, 2013; ISBN 978-0-470-90687-3.
18. Koros, W.J.; Burgess, S.K.; Chen, Z. Polymer Transport Properties. In *Encyclopedia of Polymer Science and Technology*, 4th ed.; John Wiley & Sons: Hoboken, NJ, USA, 2015; ISBN 9781118633892.
19. Koros, W.J.; Fleming, G.K.; Jordan, S.M.; Kim, T.H.; Hoehn, H.H. Polymeric membrane materials for solution-diffusion based permeation separations. *Prog. Polym. Sci.* **1988**, *13*, 339–401. [[CrossRef](#)]
20. Scherillo, G.; Petretta, M.; Galizia, M.; La Manna, P.; Musto, P.; Mensitieri, G. Thermodynamics of water sorption in high performance glassy thermoplastic polymers. *Front. Chem.* **2014**, *2*, 25. [[CrossRef](#)] [[PubMed](#)]
21. Scherillo, G.; Galizia, M.; Musto, P.; Mensitieri, G. Water Sorption Thermodynamics in Glassy and Rubbery Polymers: Modeling the Interactional Issues Emerging from FTIR Spectroscopy. *Ind. Eng. Chem. Res.* **2013**, *52*, 8674–8691. [[CrossRef](#)]
22. Scherillo, G.; Sanguigno, L.; Galizia, M.; Lavorgna, M.; Musto, P.; Mensitieri, G. Non-equilibrium compressible lattice theories accounting for hydrogen bonding interactions: Modelling water sorption thermodynamics in fluorinated polyimides. *Fluid Phase Equilib.* **2012**, *334*, 166–188. [[CrossRef](#)]
23. Musto, P. Two-Dimensional FTIR Spectroscopy Studies on the Thermal-Oxidative Degradation of Epoxy and Epoxy–Bis(maleimide) Networks. *Macromolecules* **2003**, *36*, 3210–3221. [[CrossRef](#)]

24. Panayiotou, C.; Pantoula, M.; Stefanis, E.; Tsivintzelis, I.; Economou, I.G. Nonrandom Hydrogen-Bonding Model of Fluids and Their Mixtures. 1. Pure Fluids. *Ind. Eng. Chem. Res.* **2004**, *43*, 6592–6606. [[CrossRef](#)]
25. Panayiotou, C.; Tsivintzelis, I.; Economou, I.G. Nonrandom Hydrogen-Bonding Model of Fluids and Their Mixtures. 2. Multicomponent Mixtures. *Ind. Eng. Chem. Res.* **2007**, *46*, 2628–2636. [[CrossRef](#)]
26. Doghieri, F.; Sarti, G.C. Nonequilibrium Lattice Fluids: A Predictive Model for the Solubility in Glassy Polymers. *Macromolecules* **1996**, *29*, 7885–7896. [[CrossRef](#)]
27. Sarti, G.C.; Doghieri, F. Predictions of the solubility of gases in glassy polymers based on the NELF model. *Chem. Eng. Sci.* **1998**, *53*, 3435–3447. [[CrossRef](#)]
28. Robeson, L.M. Polymer membranes for gas separation. *Curr. Opin. Solid. State Mater. Sci.* **1999**, *4*, 549–555. [[CrossRef](#)]
29. Seo, J.; Jang, W.; Han, H. Thermal, optical, and water sorption properties in composite films of poly(ether imide) and bismaleimides: Effect of chemical structure. *J. Appl. Polym. Sci.* **2009**, *113*, 777–783. [[CrossRef](#)]
30. Karimi, M.; Albrecht, W.; Heuchel, M.; Kish, M.H.; Frahn, J.; Weigel, T.; Hofmann, D.; Modarress, H.; Lendlein, A. Determination of water/polymer interaction parameter for membrane-forming systems by sorption measurement and a fitting technique. *J. Membr. Sci.* **2005**, *265*, 1–12. [[CrossRef](#)]
31. Merdas, I.; ThomINETTE, F.; Verdu, J. Humid ageing of polyetherimide. Chemical and physical interactions with water. In *Polyimides and Other High Temperature Polymer: Synthesis, Characterization and Applications*; Mittal, K.L., Ed.; VSP: Utrecht, The Netherlands, 2003; Volume 2, pp. 255–266. ISBN 90-6764-378-5.
32. Okamoto, K.-I.; Tanihara, N.; Watanabe, H.; Tanaka, K.; Kita, H.; Nakamura, A.; Kusuki, Y.; Nakagawa, K. Sorption and diffusion of water vapor in polyimide films. *J. Polym. Sci. Pol. Phys.* **1992**, *30*, 1223–1231. [[CrossRef](#)]
33. Wang, Y.; Jiang, L.; Matsuura, T.; Chung, T.S.; Goh, S.H. Investigation of the fundamental differences between polyamide-imide (PAI) and polyetherimide (PEI) membranes for isopropanol dehydration via pervaporation. *J. Membr. Sci.* **2008**, *318*, 217–226. [[CrossRef](#)]
34. Wang, Y.; Chung, T.S.; Neo, B.W.; Gruender, M. Processing and engineering of pervaporation dehydration of ethylene glycol via dual-layer polybenzimidazole (PBI)/polyetherimide (PEI) membranes. *J. Membr. Sci.* **2011**, *378*, 339–350. [[CrossRef](#)]
35. Zhao, W.; Shi, B. Removal of Volatile Organic Compounds from Water by Pervaporation Using Polyetherimide-Polyethersulfone Blend Hollow Fiber Membranes. *Sep. Sci. Technol.* **2009**, *44*, 1737–1752. [[CrossRef](#)]
36. Qiu, W.; Kosuri, M.; Zhou, F.; Koros, W.J. Dehydration of ethanol–water mixtures using asymmetric hollow fiber membranes from commercial polyimides. *J. Membr. Sci.* **2009**, *327*, 96–103. [[CrossRef](#)]
37. Huang, R.Y.M. (Ed.) *Pervaporation Membrane Separation Processes*; Membrane Science and Technology Series; Elsevier Science Publishers: Amsterdam, The Netherlands, 1991; Volume 1, ISBN 0-444-88227-8.
38. Semenova, S.I. Separation properties of polyimides. In *Polyimide Membranes-Applications, Fabrications, and Properties*; Ohya, H., Kudryavsev, V.V., Semenova, S.I., Eds.; Kodansha: Tokyo, Japan, 1996; pp. 103–178. ISBN 4-06-208189-X.
39. Feng, X.; Huang, R.Y.M. Pervaporation and performance of asymmetric polyetherimide membranes for isopropanol dehydration by pervaporation. *J. Membr. Sci.* **1996**, *109*, 165–172. [[CrossRef](#)]
40. Yanagishita, H.; Maejima, C.; Kitamoto, D.; Nakane, T. Preparation of asymmetric polyimide membrane for water/ethanol separation in pervaporation by the phase inversion process. *J. Membr. Sci.* **1994**, *86*, 231–240. [[CrossRef](#)]
41. Huang, R.Y.M.; Feng, X. Dehydration of isopropanol by pervaporation using aromatic polyetherimide membranes. *Sep. Sci. Technol.* **1993**, *28*, 2035–2048. [[CrossRef](#)]
42. Yanagishita, H.; Kitamoto, D.; Nakane, T. Separation of alcohol aqueous solution by pervaporation using asymmetric polyimide membrane. *High Perform. Polym.* **1995**, *7*, 275–281. [[CrossRef](#)]
43. Okamoto, K.; Tanihara, N.; Watanabe, H.; Tanaka, K.; Kita, H.; Nakamura, A.; Kusuki, Y.; Nakagawa, K. Vapor permeation and pervaporation separation of water-ethanol through polyimide membranes. *J. Membr. Sci.* **1992**, *68*, 53–63. [[CrossRef](#)]
44. Chen, W.J.; Martin, C.R. Highly methanol selective membranes for the pervaporation separation of methyl-t-butyl ether/methanol mixtures. *J. Membr. Sci.* **1995**, *104*, 101–108. [[CrossRef](#)]
45. Nakagawa, K.; Asakura, Y.; Nakanishi, S.; Hoshino, H.; Kouda, H.; Kusuki, Y. Separation of vapor mixtures of water and alcohol by aromatic polyimide hollow fibers. *Kobunshi Ronbunshu* **1989**, *46*, 405–411. [[CrossRef](#)]

46. De Nicola, A.; Correa, A.; Milano, G.; La Manna, P.; Musto, P.; Mensitieri, G.; Scherillo, G. Local Structure and Dynamics of Water Absorbed in Polyetherimide: A Hydrogen Bonding Anatomy. *J. Phys. Chem. B* **2017**, *121*, 3162–3176. [[CrossRef](#)] [[PubMed](#)]
47. Musto, P.; Galizia, M.; La Manna, P.; Pannico, M.; Mensitieri, G. Diffusion and Molecular Interactions in a Methanol/Polyimide System Probed by Coupling time-resolved FTIR Spectroscopy with Gravimetric Measurements. *Front. Chem.* **2014**, *2*, 1–9. [[CrossRef](#)]
48. Galizia, M.; La Manna, P.; Pannico, M.; Mensitieri, G.; Musto, P. Methanol diffusion in polyimides: A molecular description. *Polymer* **2014**, *55*, 1028–1039. [[CrossRef](#)]
49. Cotugno, S.; Larobina, D.; Mensitieri, G.; Musto, P.; Ragosta, G. A novel spectroscopic approach to investigate transport processes in polymers: The case of water–epoxy system. *Polymer* **2001**, *42*, 6431–6438. [[CrossRef](#)]
50. Mensitieri, G.; Cotugno, S.; Musto, P.; Ragosta, G.; Nicolais, L. Transport of water in high Tg Polymers: A comparison between interacting and non-interacting systems. In *Polyimides and Other High Temperature Polymers: Synthesis, Characterization and Applications*; Mittal, K.L., Ed.; VSP: Utrecht, The Netherlands, 2003; Volume 2, pp. 267–285. ISBN 90-6764-378-5.
51. Sanchez, I.C.; Lacombe, R.H. An Elementary Molecular Theory of Classical Fluids. Pure Fluids. *J. Phys. Chem.* **1976**, *80*, 2352–2362. [[CrossRef](#)]
52. Sanchez, I.C.; Lacombe, R.H. Statistical Thermodynamics of Fluid Mixtures. *J. Phys. Chem.* **1976**, *80*, 2568–2580.
53. Sanchez, I.C.; Lacombe, R.H. Statistical Thermodynamics of Polymer Solutions. *Macromolecules* **1978**, *11*, 1145–1156. [[CrossRef](#)]
54. Panayiotou, C.; Sanchez, I.C. Hydrogen Bonding in Fluids—An Equation-of-State Approach. *J. Phys. Chem.* **1991**, *95*, 10090–10097. [[CrossRef](#)]
55. Veytsman, B.A. Are Lattice Models Valid for Fluids with Hydrogen Bonds? *J. Phys. Chem.* **1990**, *94*, 8499–8500. [[CrossRef](#)]
56. Veytsman, B.A. Equation of State for Hydrogen-Bonded Systems. *J. Phys. Chem.* **1998**, *B 102*, 7515–7517. [[CrossRef](#)]
57. Prausnitz, J.M.; Lichtenthaler, R.N.; Gomes de Azevedo, E. *Molecular Thermodynamics of Fluid-Phase Equilibria*, 3rd ed.; Prentice Hall PTR: Upper Saddle River, NJ, USA, 1998; ISBN 978-0139777455.
58. Guggenheim, E.A. *Mixtures: The Theory of the Equilibrium Properties of Some Simple Classes of Mixtures, Solutions and Alloys*; Oxford University Press: Oxford, UK, 1952.
59. Panayiotou, C.; Vera, J.H. Statistical Thermodynamics of r-Mer Fluids and Their Mixtures. *Polym. J.* **1982**, *14*, 681–694. [[CrossRef](#)]
60. You, S.S.; Yoo, K.P.; Lee, C.S. An Approximate Nonrandom Lattice Theory of Fluids: General Derivation and Application to Pure Fluids. *Fluid Phase Equilib.* **1994**, *93*, 193–213. [[CrossRef](#)]
61. Taimoori, M.; Panayiotou, C. The non-random distribution of free volume in fluids: Non-polar systems. *Fluid Phase Equilib.* **2001**, *192*, 155–169. [[CrossRef](#)]
62. Yeom, M.S.; Yoo, K.P.; Park, B.H.; Lee, C.S. A Nonrandom Lattice Fluid Hydrogen Bonding Theory for Phase Equilibria of Associating Systems. *Fluid Phase Equilib.* **1999**, *158*, 143–149. [[CrossRef](#)]
63. Vlachou, T.; Prinos, I.; Vera, J.H.; Panayiotou, C. Nonrandom Distribution of Free Volume in Fluids and their Mixtures: Hydrogen-Bonded Systems. *Ind. Eng. Chem. Res.* **2002**, *41*, 1057–1063. [[CrossRef](#)]
64. Panayiotou, C. The QCHB Model of Fluids and their Mixtures. *J. Chem. Thermodyn.* **2003**, *35*, 349–381. [[CrossRef](#)]
65. Tsivintzelis, I.; Kontogeorgis, G.M. Modeling the Vapor–Liquid Equilibria of Polymer–Solvent Mixtures: Systems with Complex Hydrogen Bonding Behavior. *Fluid Phase Equilib.* **2009**, *280*, 100–109. [[CrossRef](#)]
66. Doghieri, F.; Quinzi, M.; Rethwisch, D.G.; Sarti, G.C. Predicting Gas Solubility in Glassy Polymers through Nonequilibrium EOS. In *Advanced Materials for Membrane Separations*; Pinnau, I., Freeman, B.D., Eds.; ACS Symposium ser. N. 876; American Chemical Society (ACS): Washington, DC, USA, 2004; pp. 74–90, ISBN 0-8412-3833-2.
67. De Angelis, M.G.; Doghieri, F.; Sarti, G.C.; Freeman, B.D. Modeling gas sorption in amorphous Teflon through the non equilibrium thermodynamics for glassy polymers (NETGP) approach. *Desalination* **2006**, *193*, 82–89. [[CrossRef](#)]
68. Pantoula, M.; von Schnitzler, J.; Eggers, R.; Panayiotou, C. Sorption and swelling in glassy polymer/carbon dioxide systems Part II—Swelling. *J. Supercrit. Fluid* **2007**, *39*, 426–434. [[CrossRef](#)]

69. Musto, P.; Ragosta, G.; Mensitieri, G.; Lavorgna, M. On the Molecular Mechanism of H₂O Diffusion into Polyimides: A Vibrational Spectroscopy Investigation. *Macromolecules* **2007**, *40*, 9614–9627. [[CrossRef](#)]
70. Czarnecki, M.A. Two-Dimensional Correlation Spectroscopy: Effect of Normalization of the Dynamic Spectra. *Appl. Spectrosc.* **1999**, *53*, 1392–1397. [[CrossRef](#)]
71. Noda, I.; Ozaki, Y. *Two-Dimensional Correlation Spectroscopy: Applications in Vibrational and Optical Spectroscopy*; John Wiley & Sons: Chichester, UK, 2005; ISBN 978-0-471-62391-5.
72. Musto, P.; La Manna, P.; Pannico, M.; Mensitieri, G.; Gargiulo, N.; Caputo, D. Molecular interactions of CO₂ with the CuBTC metal organic framework: An FTIR study based on two-dimensional correlation spectroscopy. *J. Mol. Struct.* **2018**, *1166*, 326–333. [[CrossRef](#)]
73. Rothshild, W.G. Mobility of Small Molecules in Viscous Media. *Macromolecules* **1968**, *1*, 43–47.
74. Stolov, A.A.; Morozov, A.I.; Remizov, A.B. Infrared spectra and spinning diffusion of methyl bromide in solutions. *Vib. Spectrosc.* **1997**, *15*, 211–218. [[CrossRef](#)]
75. Tsivintzelis, I.; Grenner, A.; Economou, I.G.; Kontogeorgis, G.M. Evaluation of the Nonrandom Hydrogen Bonding (NRHB) Theory and the Simplified Perturbed-Chain Statistical Associating Fluid Theory (sPC-SAFT). 2. Liquid-Liquid Equilibria and Prediction of Monomer Fraction in Hydrogen Bonding Systems. *Ind. Eng. Chem. Res.* **2008**, *47*, 5651–5659. [[CrossRef](#)]
76. Fredenslund, A.; Jones, R.L.; Prausnitz, J.M. Group-contribution estimation of activity coefficients in nonideal liquid mixtures. *AIChE J.* **1975**, *21*, 1086–1099. [[CrossRef](#)]
77. Sorensen, M.J. Group Contribution Estimation Methods. In *Models for Thermodynamic and Phase Equilibria Calculations*; Sandler, S.I., Ed.; Marcel Dekker: New York, NY, USA, 1994; ISBN 978-0824791308.



© 2019 by the authors. Licensee MDPI, Basel, Switzerland. This article is an open access article distributed under the terms and conditions of the Creative Commons Attribution (CC BY) license (<http://creativecommons.org/licenses/by/4.0/>).